Retrieval of Chlorophyll-a concentration and associated product uncertainty in optically diverse lakes and reservoirs

Xiaohan Liu [a,*], Christopher Steele [a,b], Stefan Simis [a], Mark Warren [a], Andrew Tyler [c], Evangelos Spyrakos [c], Nick Selmes [a], Peter Hunter [c]

[a] *Plymouth Marine Laboratory, Prospect Place, The Hoe, Plymouth PL1 3DH, United Kingdom*
[b] *Met Office, FitzRoy Road, Exeter EX1 3PB, United Kingdom*
[c] *Earth and Planetary Observation Centre, Biological and Environmental Sciences, Faculty of Natural Sciences, University of Stirling, Stirling FK9 4LA, United Kingdom*

ARTICLE INFO

ABSTRACT

Satellite product uncertainty estimates are critical for the further development and evaluation of remote sensing algorithms, as well as for the user community (e.g., modelers, climate scientists, and decision-makers). Optical remote sensing of water quality is affected by significant uncertainties stemming from correction for atmospheric effects as well as a lack of algorithms that can be universally applied to waterbodies spanning several orders of magnitude in non-covarying substance concentrations. We developed a method to produce estimates of Chlorophyll-a (Chla) satellite product uncertainty on a pixel-by-pixel basis within an Optical Water Type (OWT) classification scheme. This scheme helps to dynamically select the most appropriate algorithms for each satellite pixel, whereas the associated uncertainty informs downstream use of the data (e.g., for trend detection or modeling) as well as the future direction of algorithm research. Observations of Chla were related to 13 previously established OWT classes based on their corresponding water-leaving reflectance (R_w), each class corresponding to specific bio-optical characteristics. Uncertainty models corresponding to specific algorithm - OWT combinations for Chla were then expressed as a function of OWT class membership score. Embedding these uncertainty models into a fuzzy OWT classification approach for satellite imagery allows Chla and associated product uncertainty to be estimated without a priori knowledge of the biogeochemical characteristics of a water body. Following blending of Chla algorithm results according to per-pixel fuzzy OWT membership, Chla retrieval shows a generally robust response over a wide range of class memberships, indicating a wide application range (ranging from 0.01 to 362.5 mg/m^3). Low OWT membership scores and high product uncertainty identify conditions where optical water types need further exploration, and where biogeochemical satellite retrieval algorithms require further improvement. The procedure is demonstrated here for the Medium Resolution Imaging Spectrometer (MERIS) but could be repeated for other sensors, atmospheric correction methods and optical water quality variables.

1. Introduction

The health of the world's freshwater bodies is of vital importance to the biosphere but monitoring water quality in all estimated 117 million lakes is not possible with conventional methods (Downing et al., 2006; Dudgeon et al., 2006; Verpoorter et al., 2014). Satellite remote sensing (RS) is essential to understand aquatic ecosystems since it offers the capability for synoptic, global observation of critical physical and biogeochemical variables in a cost-effective manner (Vantrepotte et al., 2012). As a core indicator of biological water quality, chlorophyll-a (Chla) is widely used as a proxy of primary production and eutrophication helping to assess aquatic health and ecosystem functioning (Cole and Weihe, 2015; Kirk, 2011). Chla products from Earth Observation (EO) can describe variations over time and space, providing critical insight into changing trophic status and environmental stressors including associated changes in phenology (Palmer et al., 2015). This makes Chla one of the most fundamental parameters in oceanic and limnologic research, climate change studies, and aquatic ecosystem management (Boyer et al., 2009; Karydis and Kitsiou, 2019; Kromkamp and Van Engeland, 2010).

As with any EO measurand, product uncertainty forms an inherent element of aquatic remote sensing (IOCCG, 2019; Merchant et al., 2017). It is common practice in studies of ocean-colour to evaluate product uncertainty using concurrent in situ measurements at global or regional scales (Mueller and Fargion, 2002). When this comparison with in situ measurement is applied to a dataset as a whole, it provides an estimate of the overall performance of the applied methodology assessed against reference observations. Ideally, uncertainty in remotely sensed products should be evaluated on a pixel-by-pixel basis (Calmettes and Giardino, 2019; Jackson et al., 2017; Merchant et al., 2017). This implies that the methodology used to assess product uncertainty should account for variability in the remotely sensed quantity. For example, numerical ecosystem and biogeochemical models frequently involve ocean colour products for model performance evaluation, where uncertainty estimates provide context for the model-data comparison (Dutkiewicz et al., 2015; Henson et al., 2009). Data assimilation of ocean colour data and models also require a full understanding of product uncertainty (Brasseur et al., 2009; Nerger and Gregg, 2007). When water quality products derived from ocean colour are adopted in decision making, information on the uncertainty informs the level of confidence in the decision made and supports the management actions that follow. Currently, product uncertainty information is incomplete at best for optically complex waterbodies and lakes in particular. The capability to accurately predict product uncertainty is crucial in such situations to inform downstream applications, further research directions and new remote sensing capabilities.

Several sources of uncertainty should be considered for uncertainty characterization of optical water quality products such as Chla. Detector noise related to sensor calibration and long-term stability issues introduce uncertainties to the signal recorded at the top-of-atmosphere (Dinguirard and Slater, 1999). The atmosphere and the corresponding atmospheric correction procedure account for the major fraction of the product uncertainty, since more than 90% of the measured upwelling radiance in the visible band at the Top of the Atmosphere (TOA) can be scattered by the atmosphere and this information cannot be independently obtained at the same scale (Harmel and Chami, 2011). As a result, the separation of water-leaving and atmospheric radiances is highly ambiguous, particularly when dealing with an optically complex water component or adjacent land. Certain observation effects, notably the optical pathlength to the target under variable viewing and illumination angles, are expected to influence the magnitude in uncertainties from atmospheric correction of the TOA signal, affecting normalized water-leaving reflectance (R_w, dimensionless). Therefore, atmospheric correction is commonly understood to be the dominant source of error in deriving R_w (Gordon and Wang, 1992; IOCCG, 2010; Warren et al., 2019). Approaches that circumvent the atmospheric contribution by interpreting TOA or partially corrected TOA have shown effective retrieval of water quality properties from red and near-infrared wavebands, carrying Chla information in relatively turbid and productive waters (Matthews et al., 2012; Shi et al., 2014). The presence of relatively bright objects near the water target, such as clouds, snow, ice, or land introduces an adjacency effect on nearby water pixels, which is known to result in over-correction of atmospheric effects and can yield low or negative R_w (Guanter et al., 2010). Regardless of their source, uncertainties in the R_w products are subsequently propagated to any derived water quality products (e.g., Chla) depending on specific algorithm sensitivities to the observed effects.

The present study is undertaken as part of the Lakes_cci project (ESA Climate Change Initiative), which aims to provide a multi-decadal, multi-sensor, and global (2000 lakes) climate data record of R_w and optical-biogeochemical water quality products. To fulfill requirements for product uncertainty characterization, both to be consistent with other satellite-observed climate data records and to meet user requirements (Calmettes and Giardino, 2019), our objective is to add per-pixel uncertainty estimates to *Calimnos,* a multi-sensor water quality processing chain configured for inland waterbodies (Simis et al., 2020b).

Calimnos uses dynamic algorithm selection and blending based on the per-pixel similarities of R_w to a set of Optical Water Types (OWTs) commonly found in natural water bodies (Spyrakos et al., 2018), as explained below. The main challenge of this work is the relative scarcity of independent in situ validation data for the target products and R_w in particular, and the uneven distribution of in situ reference data across the identified OWTs. While it would be desirable to derive an uncertainty budget for all sources of uncertainty, we do not consider this feasible at present. Our focus is therefore on the uncertainty characterization of the final Chla product in relation to OWT classification.

Assessing the optical properties of 2000 lakes implies that a priori knowledge of the (varying) inherent optical properties of the observed waterbody cannot be assumed, because of the optical diversity and complexity of inland waterbodies (Kirk, 2011; Liu et al., 2013; Morel and Prieur, 1977). Unlike clear oceanic waters where the concentrations of water constituents (pigments, suspended material, and coloured dissolved organic matter) may be assumed to covary with Chla, optically complex waters can see any substance dominate and vary independently, particularly near terrestrial sources or in shallow waters (Kirk, 2011; Morel and Prieur, 1977). Algorithms that retrieve water constituent concentrations are commonly designed and validated for a specific optical water type, concentration range, dataset, or region. For example, the retrievals of OCx blue-green band ratio algorithms proposed by NASA will show a linear response to Chla in relatively clear waters where absorption is dominated by phytoplankton (O'Reilly et al., 2000), while algorithms based on NIR-red ratios are more applicable in turbid productive waters where coloured dissolved organic matter and suspended material efficiently absorbs blue light (Moses et al., 2019; Neil et al., 2019). The optical complexity of inland waters, therefore, limits the applicability of such algorithms to optically diverse waterbodies, and algorithm performance is expected to be less accurate when it is applied to a region or water type outside of the validated scope. By associating candidate algorithms only with specific optical signatures, out-of-scope algorithm assignment can be avoided. This has been demonstrated in the case of switching algorithm assignment for Chla in lakes (Matthews et al., 2012) and can be further harmonized by blending the response of multiple candidate algorithms in edge cases, as demonstrated for ocean applications (Jackson et al., 2017). These approaches require close attention to algorithm selection and optimization whenever new water types are recognized, new sensors are introduced, or when atmospheric correction procedures are updated. While these steps add complexity, they have thus far shown a much wider range of applicability compared to single-algorithm procedures. In theory, any combination of atmospheric correction, Chla retrieval, or combined approach could be introduced in a global processing scheme based on optical water types. As such, parallels can be drawn with data-driven methods, particularly with recent advances in machine learning that have demonstrated wide applicability to inland waters (Cao et al., 2020; Kravitz et al., 2021; Pahlevan et al., 2020). However, the generalization of these method remains to be demonstrated as robust across water types, atmospheric conditions and seasonality (noting the relevant issue of limited availability and bias in the in situ data) and, while of similar complexity, the assignment of individually validated algorithms to optical water types has the potential to provide a more transparent understanding of optical behaviours of waterbodies, including the characterization of product uncertainty.

We hypothesize that the uncertainties associated with selecting appropriate retrieval algorithms can be somewhat better managed by introducing an Optical Water Type (OWT) classification procedure prior to the application and assignment of bio-optical algorithms, following a series of recent developments to characterize these in natural waters (Moore et al., 2014; Shi et al., 2013; Spyrakos et al., 2018; Spyrakos et al., 2011; Vantrepotte et al., 2012). A remaining challenge is that in situ reference observations are relatively scarce and not equally distributed across optical water types: waterbodies suffering the effects of eutrophication have been studied far more than relatively clear water

bodies (Spyrakos et al., 2018). The effects of this discrepancy are potentially two-fold: first, well-studied environments will likely have better suited and performing algorithms. Second, product uncertainties for well-studied environments tend to be lower and derived with more confidence. An element of uncertainty should thus be expected even in the assessment of product uncertainty itself, for less-studied environments. The OWT framework helps here to pool together the available in situ calibration and validation data from waterbodies that cluster under the same OWT, regardless of sampling location.

In summary, to further the development of aquatic remote sensing products in optically diverse inland waters, this study introduces a methodology for quantification of product uncertainties within an OWT-based algorithm assignment framework. Based on 13 OWT classes identified from a large global database of in situ water-leaving reflectance by Spyrakos et al. (2018), and initial algorithm selection and assignment work within the OWT framework conducted by Neil et al. (2019), we identify the following individual steps to reach this goal: (1) assessment of biases in the retrieval of satellite R_w against any available in situ observations, irrespective of OWT; (2) adopting the tuning of candidate algorithms suggested by Neil et al. (2019) against an extensive dataset of Chla measurements, and an initial validation step to map suitable algorithms to given OWTs; (3) using a fuzzy OWT classification procedure to weight individual algorithm results using the membership scores (S_{OWT}) for 13 OWT classes, followed by weighted averaging to provide a blending Chla product; (4) Assessing performance of the individual algorithms and the blended algorithm result, expressing the statistical uncertainty as a function of S_{OWT}. Finally, (5) the OWT-specific uncertainty functions are combined to allow pixel-wise application, taking only S_{OWT} as input. We note that steps 1–2 do not include a new round-robin comparison of algorithm performance, and this study is specific to the selected algorithms and atmospheric correction pre-processing. It is, however, expected that this procedure to derive product uncertainties is equally applicable to different correction schemes and combinations of algorithms, which result from future algorithm comparisons. It is further noted that this integrated approach is developed entirely with in situ matchups corresponding to satellite imagery of the Medium Resolution Imaging Spectrometer (MERIS), which to date benefits the largest volume of in situ data shared within the scientific community. We demonstrate the resultant Chla products and products uncertainties for a number of optically varied water bodies, and extend the application of the processing system to the Ocean and Land Colour Instrument (OLCI) onboard the Sentinel-3 satellites, which carries a similar optical configuration.

2. Data and methods

2.1. In situ and satellite data

2.1.1. In situ data

In situ observation data for this study were sourced from the in situ bio-optical

data repository LIMNADES (Lake Bio-optical Measurements and Matchup Data for Remote Sensing: http://www.limnades.stir.ac.uk), which comprises 25 individual datasets collected from over 200 inland water bodies across the globe (Table 1). This included 1982 individual observations of remote-sensing reflectance ($R_{rs} = L_w(0^+)/E_d(0^+)$, sr^{-1}, where L_w and E_d are the water-leaving radiance and total downwelling irradiance evaluated just above the water, respectively) and 28,726 observations of Chla concentration (mg/m^3). From this archive, 288 R_{rs} and 2616 Chla observations had concurrent satellite matchups with MERIS, operating in the period 2002–2012 (Fig. 1, see section 2.1.2). The in situ R_{rs} were converted to water-leaving reflectance (assuming $R_w = R_{rs} \times \pi$) to facilitate comparison between in situ and satellite measurements. The Chla matchup datasets showed a wide concentration range from 0.01 to 365.5 mg/m^3, covering oligotrophic to hypereutrophic waters (Table 1 and Fig. 2). Table 1 shows a summary of the

Table 1

Summary of the chlorophyll-a matchup datasets used in this study.

	Waterbodies	Number of matchups	Dataset identifier[a]
1	Lake Taihu (China)	45	A
2	Garda; Maggiore; Idro; Mantova; Trasimeno (Italy)	82	C
3	43 lakes in US	1376	D
4	Erie; Ontario; Winnipeg (Canada)	196	E
5	Theewaterskloof, Loskop and Zeekoevlei reservoirs	5	I
6	Fremont State Lakes (US) and Lake Kinneret (Israel)	14	M
7	Lake Balaton and 4 neighbouring aquatic systems (Hungary) Loch Leven; Loch Lomond; Windemere; Bassenthwaite; Derwand water (UK)	29	N
8	Lake Peipsi (Estonia)	9	O
9	Lough Neagh (UK)	110	[b]
10	Lake Balaton (Hungary)	431	[b]
11	Lake Balaton (Hungary)	312	[b]
12	Lake Pyhäjärvi and Lake Päijänne (Finland)	7	[b]
	Total number of matchups	2616	

[a] Dataset identifiers labeled in Alphabet (A-O) correspond to datasets as in Spyrakos et al. (2018).

[b] Datasets 9 to 12 were contributed by the institutions of Agri-food and Biosciences Institute in Northern Ireland, Balaton Limnological Institute, Hungarian Government, and Finnish Environment Institute, respectively.

Chla matchup datasets used. A detailed description of the datasets (1 to 8 as shown in Table 1) and corresponding measurement and processing protocols are provided in Spyrakos et al. (2018). Because the datasets are contributed to LIMNADES from multiple sources, it is noted that these data inevitably carry uncertainties associated with the collection and handling of water samples, instrument calibration, and environmental conditions of sampling or instrument deployment. In this study, the uncertainty estimates were based on a comparison between field data and satellite products; this end-to-end characterization of uncertainty is widely employed in ocean colour studies (IOCCG, 2019) and addresses user requirements to base uncertainty estimates on field data (Calmettes and Giardino, 2019). The nature of the end-to-end approach means that attribution of uncertainty to individual components is not directly possible, although we do present separate characterization of the retrieval of water-leaving reflectance versus the biogeochemical products derived from reflectance.

2.1.2. Satellite data

Level 1b data for MERIS (3rd reprocessing) and OLCI-A/B were obtained from the European Space Agency (ESA) for the period of 2002–2012 and 2016–2019, respectively. MERIS data were radiometrically corrected using the ESA Sentinel Application Platform (SNAP v7.0). Unsuitable data were masked based on a combination of Level-1 quality flags and results from the Idepix classifier (version 7.0). Specifically, data were removed when either of the following flags were raised: cosmetic, duplicated, glint risk, suspect, land/ocean, bright, coastline and invalid pixels from the Level1 quality flags; and invalid, cloud (including ambiguous, sure, 2-pixel buffer, and cloud shadow), snow/ice, bright, white, coastline, land, and glint risk from Idepix. Atmospheric correction was performed with POLYMER v4.12 (Steinmetz et al., 2011). This and other atmospheric correction algorithms were previously compared, including MEGS8.1 (MERIS standard), FUB, CoastColour, Case2Regional, SCAPE-M and POLYMER, as detailed in the ESA Lakes CCI Algorithm Theoretical Basis Document (Simis et al., 2020a). In summary, POLYMER was selected for its statistically most robust retrieval of R_w particularly with respect to linearity, relative errors, and number of valid retrievals. Whilst all tested algorithms produced significant biases, POLYMER showed the most systematic response, suggesting that algorithms for the retrieval of water
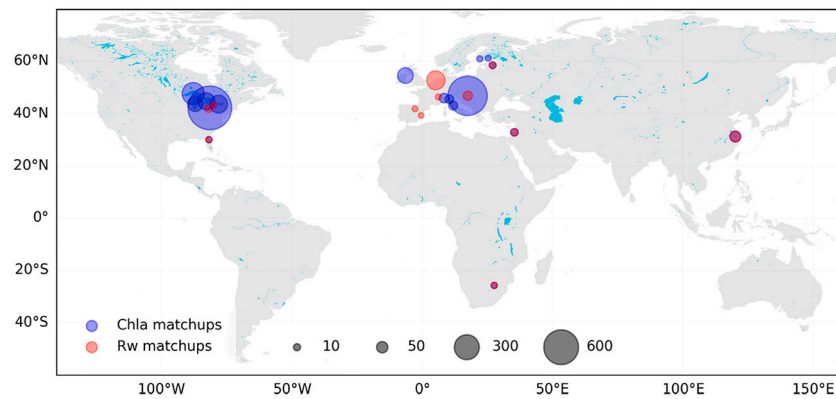
Fig. 1. Distribution of the in situ and satellite matchups for water-leaving reflectance and chlorophyll-a. Blue circles represent chlorophyll-a matchups and red circles represent reflectance matchups. The size of the circles represents the number of matchups over the 2002–2012 period. (For interpretation of the references to colour in this figure legend, the reader is referred to the web version of this article.)
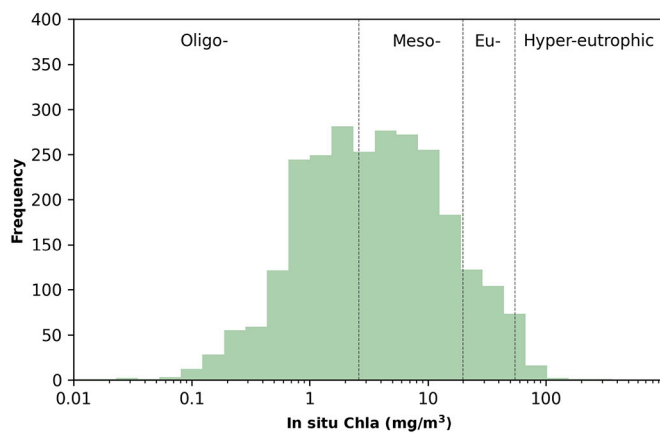

Fig. 2. Frequency distribution of chlorophyll-a concentration in the matchup datasets. Trophic states are indicated according to Carlson and Simpson (1996).

Table 2
Lakes selected as use cases.

Lake Name (latitude, longitude)	Continent	Area (km^2)	Description
Lake Taihu (31.21, 120.24)	Asia	2338	Highly eutrophic lake, with frequent phytoplankton blooms in spring and summer.
Lake Turkana (3.78, 36.05)	Africa	7566	Turbid eutrophic lake. The world's largest permanent desert lake, characterized by a strong gradient of turbidity from North to South.
Lake Vänern (59.05, 13.59)	Europe	5650	Mesotrophic lake. The largest lake in Sweden and the third largest in Europe.
Lake Vättern (58.55, 14.71)	Europe	1888	Oligotrophic clear lake. Sweden's second largest lake, deep and nutrient poor.

constitutes could be tuned to overcome such bias to retrieve accurate concentration estimates.

A comparison of satellite and in situ matchup windows showed that the number of matchups increased from 160 to 288 and from 1204 to 2616 for R_w and Chla, respectively, between temporal matchup windows of ±1 and ± 3 days, respectively (using 3 × 3 pixel windows). It was then confirmed that temporal window length (±1 and ± 3 days) had little impact on validation statistics for R_w and Chla between in situ and satellite observations (see Figs. S1 and S2 in supplementary materials). The wider temporal window was thus selected to reduce the risk of having too few matchups for less common OWTs and to generate meaningful product uncertainty metrics. The mean R_w value for each matchup was calculated from the macro-pixel for the MERIS overpass most closely matching the in situ observation time. If the same MERIS pass was found to be a valid matchup for multiple in situ observations from the same location, only the in situ value nearest in time was selected for the matchup.

Four lakes were selected to demonstrate the retrieval of Chla and corresponding per-pixel uncertainty due to their diverse optical properties and eutrophic states: Lake Taihu (highly eutrophic), Lake Turkana (turbid eutrophic), Lake Vänern (mesotrophic), and Lake Vättern (oligotrophic). A brief description of the four lakes can be found in Table 2. Cloud-free MERIS scenes covering Lakes Taihu (31 July 2010), Turkana (1 August 2011), Vänern (16 July 2006), and Vättern (16 July 2006) were used to produce example maps of Chla product uncertainty, which is the combined result of both atmospheric correction and downstream algorithm uncertainties, as well as uncertainty in the in situ

data. A consistency assessment between MERIS (2009–2011) and OLCI (2017–2019) on the blended Chla and its associated uncertainty product was performed over the four lakes to show that the approach does indeed transfer (whilst we cannot presume the lakes haven't changed).

2.2. Chla retrieval algorithm selection, optimization, and blending

Water constituent retrieval algorithms were previously selected from 19 candidate algorithms (including three blue-green band ratio algorithms, eight near infra-red and red band ratio algorithms, two peak height algorithms, five semi-analytical algorithms, and one neural network algorithm) and optimized for MERIS against the LIMNADES global in situ data set, following the procedures detailed in Neil et al. (2019). The 19 algorithms cover the vast majority of the previously published and validated algorithm forms for MERIS, and can all be applied to OLCI. Algorithms that used the same algebraic formulation but with different parameterization were not included because they would result in the same parameterization following the retuning of coefficients. Neil et al. (2019) suggested, based on analysis of algorithm response from in situ reflectance data (a larger data set than possible from satellite matchups) using a scoring system involving seven error metrics (including root mean square error, mean absolute error, slope and intercept of linear regression, Pearson's correlation coefficient, average absolute percentage difference, bias, and percentage of retrievals), that a combination of four tuned algorithms could adequately estimate Chla for a concentration range spanning three orders of magnitude (see Table 3 and Table 4 below). The selected Chla retrieval algorithms are the semi-analytical near infra-red and red band ratio algorithm by Gons et al. (2005) (denoted Gons05), the NASA OC2

Table 3
Optical water types and their descriptions after Spyrakos et al. (2018).

OWT	Description
1	Hypereutrophic with cyanobacterial scum. Very high Chla, phycocyanin, and CDOM
2	Marginal pigment and CDOM dominance over inorganic suspended particles. Balanced influence of Chla, CDOM, and inorganic suspended matter (ISM) on the optical properties
3	Clear water. Very low Chla and total suspended matter (TSM), with high Secchi depth
4	Turbid water with high coloured organic matter content. High TSM and CDOM concentration
5	Sediment-laden water. Highest ISM and low Secchi depth
6	Balanced effects of optically active constituents at shorter wavelengths. Balanced influence of Chla, CDOM, and inorganic suspended matter (ISM) on the optical properties, with moderate high concentration of phycocyanin
7	Phytoplankton-dominated waters with high cyanobacteria abundance and elevated reflectance in the red/infrared region. High Chla and phycocyanin concentration
8	Phytoplankton-dominated water with cyanobacteria abundance and a reflectance peak close to 700 nm. Very high Chla and phycocyanin, with high ISM
9	Similar to OWT 2 but with higher reflectance at shorter wavelengths. Bio-optical properties similar to OWT2, with slightly lower CDOM and ISM
10	CDOM-rich water
11	CDOM-rich water with cyanobacteria presence and high absorption efficiency by non-pigmented particulates. High CDOM and ISM
12	Turbid water with moderate phytoplankton abundance and a cyanobacteria presence. Very high ISM
13	Very clear (blue) water. The lowest Chla and TSM, with high Secchi depth

Table 4
Mapping of Chlorophyll-a algorithms to Optical Water Types, with tuned algorithm coefficients. See Appendix A for algorithm descriptions.

Algorithm	Optical Water Type number	Tuned Parameters[a]
OC2 (https://oceancolor.gsfc.nasa.gov/atbd/chlor_a/)	3, 9, 10, 13	a0 = 0.1731, a1 = −3.9630, a2 = −0.5620, a3 = 4.5008, a4 = −3.0020
708/665 empirical band ratio based on Gilerson et al. (2010)	2, 8, 11, 12	A = 79.62, B = 0.7393, C = −54.99
Semi-analytical NIR-Red band algorithm for MERIS based on Gons et al. (2005)	1, 4, 5, 6	$a^*_{ph}(665) = 0.025$
Adapted QAA algorithm according to (Mishra et al., 2013a; Mishra et al., 2013b)	7	$S_{CDOM} = 0.0135$

[a] It is noted that while the methodology of algorithm tuning is as described in Neil et al. (2019), tuned coefficients differ since the former were derived from in situ reflectance data against LIMNADES while this study uses coefficients optimized for POLYMER-corrected satellite reflectance.

algorithm (O'Reilly et al., 1998), an empirical red near infra-red band ratio algorithm similar to Gilerson et al. (2010) and here denoted R708/R665, and two adaptations of the Quasi-Analytical Algorithm (QAA) (Lee et al., 2014; Mishra et al., 2013a; Mishra et al., 2013b). A brief description of these algorithms can be found in the Appendix. In this study, independent validation of the algorithms is not feasible, since the algorithms adopted from the procedure described by Neil et al. (2019) have already used the same source of in situ data so this would have large overlap with this evaluation.

In this study, a blending procedure based on OWT similarity scores is used to create a continuous Chla response across water types and concentration range. Table 3 shows a brief description of the 13 OWTs identified by Spyrakos et al. (2018) which used the gap statistic (Tibshirani et al., 2001) to select the statistically optimal number of clusters. This work was done against the same in situ dataset (LIMNADES) as used in the present study. Table 4 shows which algorithms are used for each of the 13 OWTs.

In contrast to OWT mapping used in other OWT classification based

studies (Eleveld et al., 2017; Moore et al., 2009; Moore et al., 2014; Vantrepotte et al., 2012), this study adopts the spectral angle (Kruse et al., 1993) rather than *Mahalonobis distance* as metric for the similarity between observed and reference OWT spectra. This was chosen because the latter metric fails to provide results when covariance between adjacent wavebands is very low. In previous studies, the distance metric was calculated for ocean and coastal waters using a relatively small reflectance band set. Considering the wide optical diversity of inland waters, we have opted here for a simpler metric that can be used with additional wavebands and across all OWTs. A further difference with previous work is that the distance metric is calculated on standardized spectra (by converting the integrated reflectance to one for each spectrum), which emphasizes differences in spectral shape between the OWTs and reduces the influence of reflectance amplitude. To illustrate the difference between the two classification methods, OWT classifications using *Mahalanobis distance* were conducted with temporal window size of 3 days and 3 × 3 pixel windows on the same dataset. Four of the optical water types resulted in zero classifications, and another had fewer than 200, meaning that 5 out of the 13 OWTs were underrepresented (Fig. 3). In contrast, the spectral angle classification method provides a similarity score with each OWT for every sample (Fig. 3 and Fig. 9, noting that only matchups with $S_{OWT} > 0.8$ are shown in Fig. 3). This approach also ensures that the uncertainty model captures the change of uncertainty with increasing OWT class membership, which is ultimately how the per-pixel uncertainty is generated.

The spectral angle between a pixel spectrum and a reference spectrum was calculated as:

$$\alpha = cos^{-1} \frac{\sum_{i=1}^{n} p_i r_i}{\sqrt{\sum_{i=1}^{n} p_i^2} \sqrt{\sum_{i=1}^{n} r_i^2}} \quad (1)$$

$$S_{OWT} = 1 - \alpha/\pi \quad (2)$$

where p_i is the per-pixel reflectance in band i for a pixel, and r_i is the reference spectrum reflectance in band i, and α is the spectral angle between the per-pixel and reference spectrum, measured in radians. The resulting OWT membership score (S_{OWT}) has ranged from 0 to 1, where 1 implies identically shaped spectra.

A weighted blending procedure based on the S_{OWT} was adopted to generate a blended Chla product thereby reducing the uncertainty introduced by the complex optical properties of inland waters. The tuned Chla algorithms were mapped to individual pixels from the OWTs with the three highest S_{OWT} for that pixel. The algorithm results corresponding to those three OWTs were averaged using the S_{OWT} as weighting factor, after normalizing the scores between zero and one where one is the highest score and zero is the score of the 4th ranking OWT. The normalization step is necessary because the spectral angle similarity distance metric varies over a relatively narrow range (reflectance spectra of water are never highly dissimilar), which could result in relatively equal spreading of weights even when one of the underlying algorithms could be operating near the limit of its applicable range.

2.3. Per-pixel uncertainty mapping

2.3.1. Uncertainty metrics
The uncertainty metrics generated in this study include the Root Mean Squared difference (RMS), Normalized Root Mean Squared difference (NRMS), Bias and Absolute Relative Uncertainty (ARU), which are defined as follows:

$$RMS = \sqrt{\frac{1}{n} \sum_{i=1}^{n} (x_{sat} - x_{is})^2} \quad (3)$$
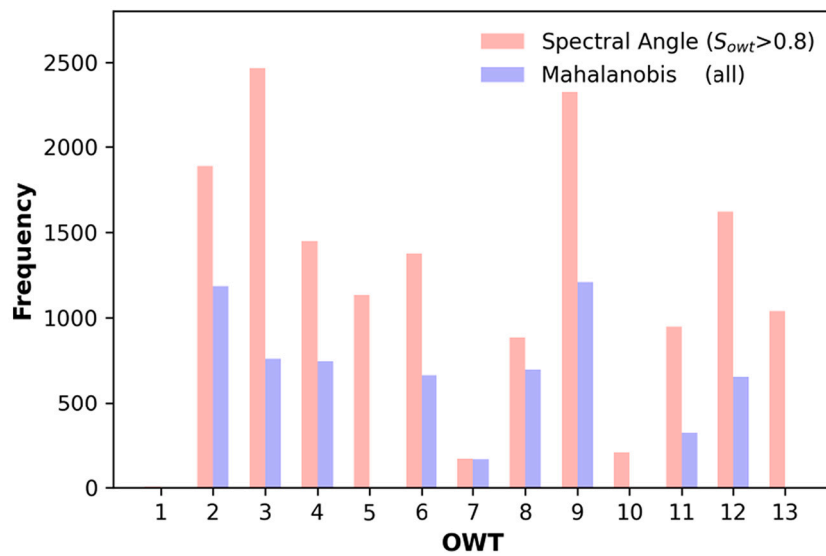
Fig. 3. Number of matchups corresponding to each optical water type (OWT) obtained using spectral angle (OWT membership scores greater than 0.8 shown) and *Mahalanobis distance* as similarity metric.
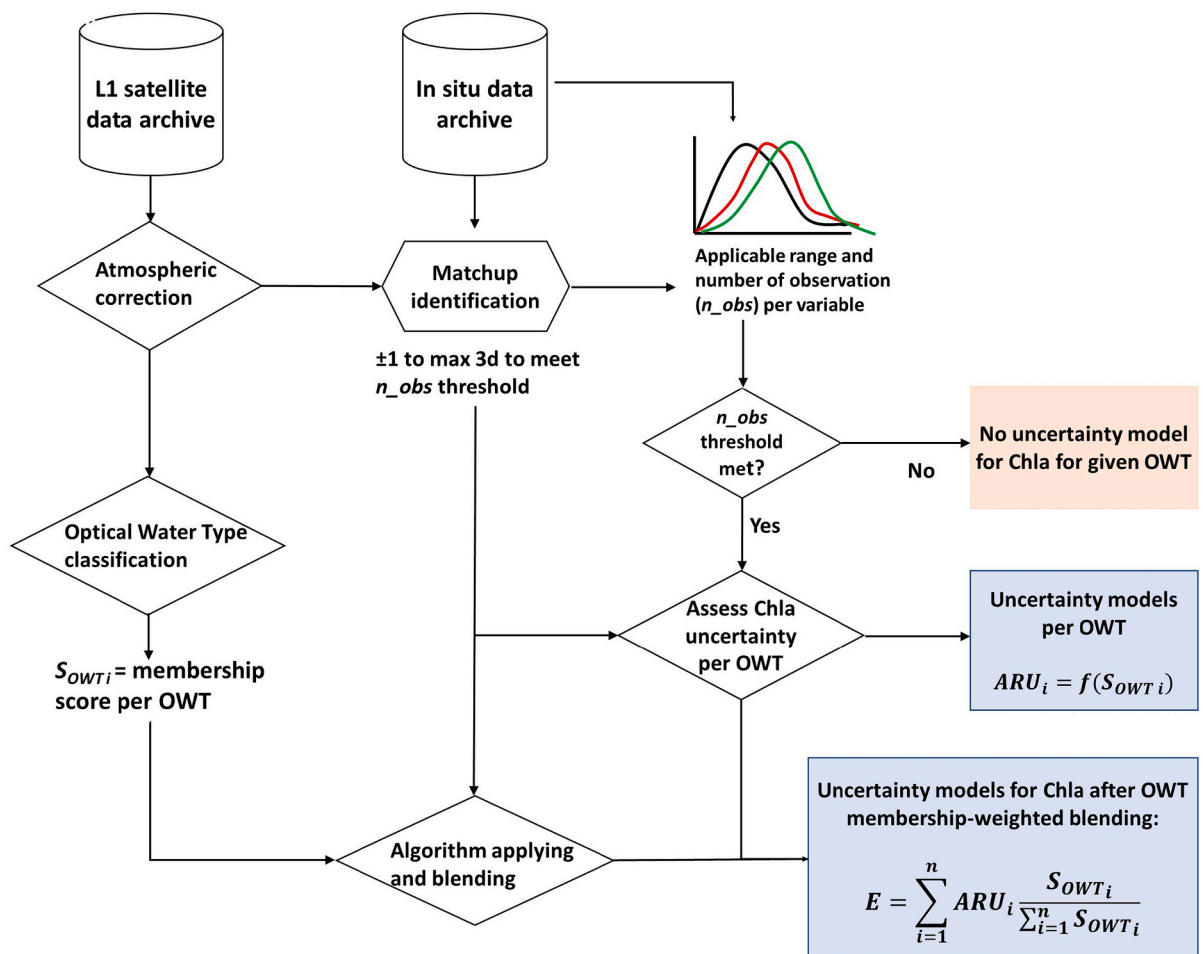

Fig. 4. Flow chart of the end-to-end assessment of chlorophyll-a products against in situ observations, resulting in uncertainty models to propagate uncertainty of the blended algorithms to each pixel.

$$NRMS = \frac{\sqrt{\frac{1}{n}\sum_{i=1}^{n}(x_{sat}-x_{is})^2}}{\frac{1}{n}\sum_{i=1}^{n}x_{is}} \cdot 100\% \qquad (4)$$

$$Bias = x_{sat} - x_{is} \qquad (5)$$

$$ARU = \left|\frac{Bias}{x_{is}}\right| \cdot 100\% \qquad (6)$$

where x_{sat} is the value derived from satellite observation and x_{is} is the value of the in situ observation, n is the total number of matchups.

In addition, the Unbiased Mean Absolute Percentage difference (UMAP) is introduced specifically for R_w validation:

$$UMAP = \frac{1}{n}\sum_{i=1}^{n}\frac{|UD_i|}{x_{is}} \qquad (7)$$

Where the Unbiased Difference (UD) is defined as the distance between the satellite R_w and the regression line (between all in situ and satellite R_w matchups). This is done to remove systematic effects from the R_w uncertainty estimate which is relevant to inform the influence of uncertainty in R_w on downstream algorithms which have been individually calibrated (as with downstream Chla algorithms). The linear regression (Y) between in situ and satellite R_w matchups at each waveband can be written as:

$$Y = a*x_{is} + b \qquad (8)$$

where a and b are the linear regression coefficients. The UD is then obtained by subtracting Y from the satellite R_w.

2.3.2. Per-pixel uncertainty propagation

A flow-chart of the procedure described here is given in Fig. 4. A series of models were generated to describe product uncertainty as a function of S_{OWT}, where each OWT was evaluated against the full matchup dataset available for the observation period of the satellite sensor. Since the full matchup dataset was used to evaluate algorithm performance for each OWT, the model can capture poor algorithm performance where the algorithm operates outside of its applicable range of OWTs, as well as the best-known performance for OWTs for which it was intended. Because each algorithm is included in the blended Chla product of a limited set of OWTs (see Table 4), the models are expected to show decreasing error estimates with increasing S_{OWT} for a subset of the OWT-specific uncertainty propagation models. The full matchup dataset was used in the modeling because OWT membership is based on conditional probabilities, which means one observation belongs to multiple classes with varying degrees of similarity. Uncertainty models can thus be formulated for OWTs which have relatively scarce representation in the matchup dataset. For a specific OWT i, a linear regression model provides the ARU uncertainty of this algorithm - OWT combination as

$$ARU_i = aS_{OWTi} + b \qquad (9)$$

where a and b are the slope and intercept of the linear fit between the chosen uncertainty metric and S_{OWTi}, the OWT membership score for this OWT calculated following eqs. (1) and (2). Because validation against an independent data set is still considered unfeasible due to the scarcity of suitable match-up data, a leave-one-out cross-validation (LOOCV) was performed on the whole dataset for each OWT to evaluate the robustness and accuracy of the proposed models. The details on the LOOCV and the distribution of mean-absolute-percentage error (MAPE) for each OWT can be found in supplementary materials (Fig. S3).

Subsequently, to compute Chla product uncertainty for each satellite observation, the OWT-specific uncertainty models associated with each of the selected algorithms are weighted in the same fashion as the blended Chla product (see section 2.2). This computation includes the

sum of each of the top-3 OWT uncertainties (ARU_i) multiplied by S_{OWT} for that OWT, relative to the sum of membership scores of the number of classes considered (M, here $n = 3$, in order of class membership), yielding the final per-pixel uncertainty E:

$$M = \sum_{i=1}^{n} S_{OWT_i}$$

$$E = \sum_{i=1}^{n} ARU_i \frac{S_{OWT_i}}{M} \qquad (10)$$

Lower and upper boundaries of the applicable range of the uncertainty model for each OWT were determined by first calculating the 1th and 99th percentile of the S_{OWTi}, and then multiplied them by 0.8 and 1.2, respectively. It is noted that the lower/upper boundaries were not simply determined as the minimum/maximum value of the S_{OWTi}, this is done to avoid the influence of extreme outliers on the determination of the application range. On a satellite Chla product uncertainty map, when the S_{OWT} of a pixel is not in the defined application range, this pixel will be flagged as having unknown product uncertainty.

3. Results

3.1. Validation of the water-leaving reflectance

Product uncertainty for normalized water-leaving reflectance was assessed from POLYMER-corrected MERIS R_w matchup results with in situ R_w at 11 wavebands from 412 nm to 779 nm, resulting in 270–288 matchups from up to 10 LIMNADES data sources, dependent on waveband. Significant linear relationships were found between the MERIS and in situ R_w (Fig. 5), with the highest coefficient of correlation (R) of 0.86 returned in the 560 nm band, and the lowest R returned of 0.47 in the 779 nm band. The NRMS was found to be higher in the shorter and longer wavebands, with NRMS of above 100% for bands of 412, 443, 754, and 779 nm. Systematic underestimation of MERIS R_w was observed for all wavebands with Bias ranging from −0.025 in the 754 nm to −0.093 in the 560 nm. The UMAP, which indicates the difference between MERIS and in situ matchups after removing the systematic effects, shows the best result as 21% at 560 nm, followed by 26%, 31%, and 31% of wavebands 510, 490, and 620 nm.

3.2. Chlorophyll-a algorithm performance per OWT

The median Chla value in each OWT for the 90th percentile of S_{OWT} ranged from 0.7 mg/m^3 for OWT 13 to 30.3 mg/m^3 for OWT 6 (Table 5), where OWT 13 represents very clear water and OWT 6 is a broad category representing balanced absorption by the various optically active water constituents (Table 3, after Spyrakos et al. (2018)). The median Chla concentration for OWT 3 was 2.4 mg/m^3, which is consistent with the definition of relatively clear water. The median Chla concentration was over 25 mg/m^3 for OWTs 1, 6, 7, and 8, all of which were originally classified as productive waters. It is noted that OWTs 1 and 7 were relatively poorly represented from the data set (low S_{OWT}, Fig. 3 and Fig. 6), indicating that these cases are less likely to have matchups in the data set or they are not well captured after atmospheric correction.

The performance of individual algorithms with their configuration as listed in Table 4 is shown for the full in situ matchup dataset in Fig. 6, with the predominant OWT for each matchup indicated by different colours. The tuned OC2 algorithm shows an even distribution around unity albeit with the highest NRMS of all four algorithms at 172% (Fig. 6a). Saturation of the OC2 algorithm appears at concentrations >10 mg/m^3. The other algorithms showed a general overestimation at low Chla values and underestimation at higher Chla values (Fig. 6b-d). The highest R of 0.67 and lowest NRMS of 36% were returned by the QAA among the four algorithms (Fig. 6d). As expected, none of the algorithms perform well over the full concentration range. The
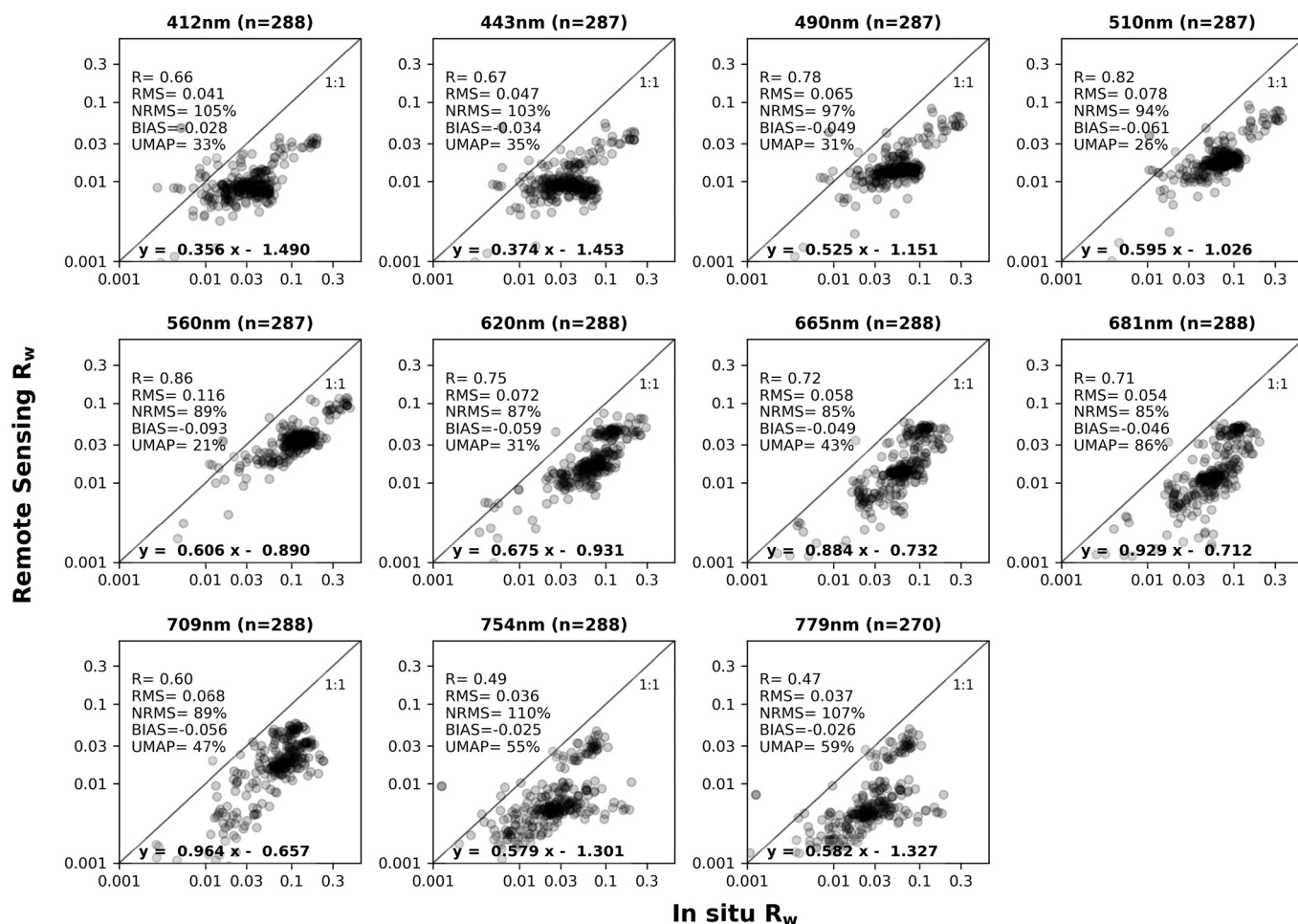
Fig. 5. Comparison between MERIS-derived and in situ R_w in each band. Scatterplots are shown in log-log scale, and the number of valid matchups (shown as *n*) depends on the in situ radiometric instruments used.

Table 5
Median, minimum, and maximum chlorophyll-a in the dataset where the OWT score was at or above the 90th percentile.

OWT	1	2	3	4	5	6	7	8	9	10	11	12	13
Median Chla (mg/m^3)	28.9	13.3	2.4	14.4	19.6	30.3	29.7	28.9	6.4	22.2	18.4	18.0	0.7
Minimum Chla	0.5	1.1	0.2	0.7	0.5	0.7	0.5	0.7	0.2	0.5	1.1	0.7	0.01
Maximum Chla	362.5	45.9	15.6	66.4	99.0	175.9	362.5	175.9	24.3	175.9	98.9	99.0	13.0

intersections of the regression fit with unity occur at 11.55, 3.94, and 4.05 mg/m^3 for R708_R665, Gons05, and QAA, respectively, suggesting they perform adequately over specific parts of the full concentration range.

Following the blending procedure described in section 2.2, the satellite retrieved Chla from the four input algorithms were mapped and blended according to the per-pixel S_{OWT} (Fig. 7). The comparison between in situ and blended Chla shows (as expected) improvements in performance, confirming the tuning and subsequent assignment of each algorithm to a subset of the concentration range and individual OWTs (Fig. 7), the regression line is close to unity, with an R of 0.83 and NRMS of 78%, both measured in log space. Fig. 8 shows the weighting factors of each algorithm in the blended Chla product, among which only the OWTs with the top-3 S_{OWT} are involved in the blending procedure. Based on in situ reflectance and pigment data analysis, Neil et al. (2019) concluded based on concentration estimates from in situ reflectance that the QAA algorithm in its tuned form is specifically applicable to OWT 7 which is associated with waters with particularly high Chla concentration and cyanobacteria abundance. We found that OWT 7 was not

assigned high S_{OWT} against any of the MERIS data processed with POLYMER in the present satellite matchup dataset. Therefore, only the weighting factors of the OC2, R708_R665, and Gons05 are included in Fig. 8 as colour coding. The weighting factors of OC2 were highest in the low Chla concentration range, and decreased with increasing Chla concentration (Fig. 8a). In contrast, the weighting factors for R708_R665 and Gons05 were found to increase with increasing Chla concentration, and the weighting factors for these two algorithms were approximately 0 for Chla <1 mg/m^3 (Fig. 8a and b).

3.3. OWT-specific uncertainty models

The relation between ARU and OWT classification scores are shown in Fig. 9 for the blended Chla product. Linear relationships were found between ARU metrics and S_{OWT} for each OWT using matchup data for the entire MERIS observation period. The majority of the OWTs show a slight decreasing trend of ARU with increasing S_{OWT}, suggesting that each R_w spectrum corresponds to at least one suitable OWT-algorithm combination. The exception is OWT 13 for which ARU overall
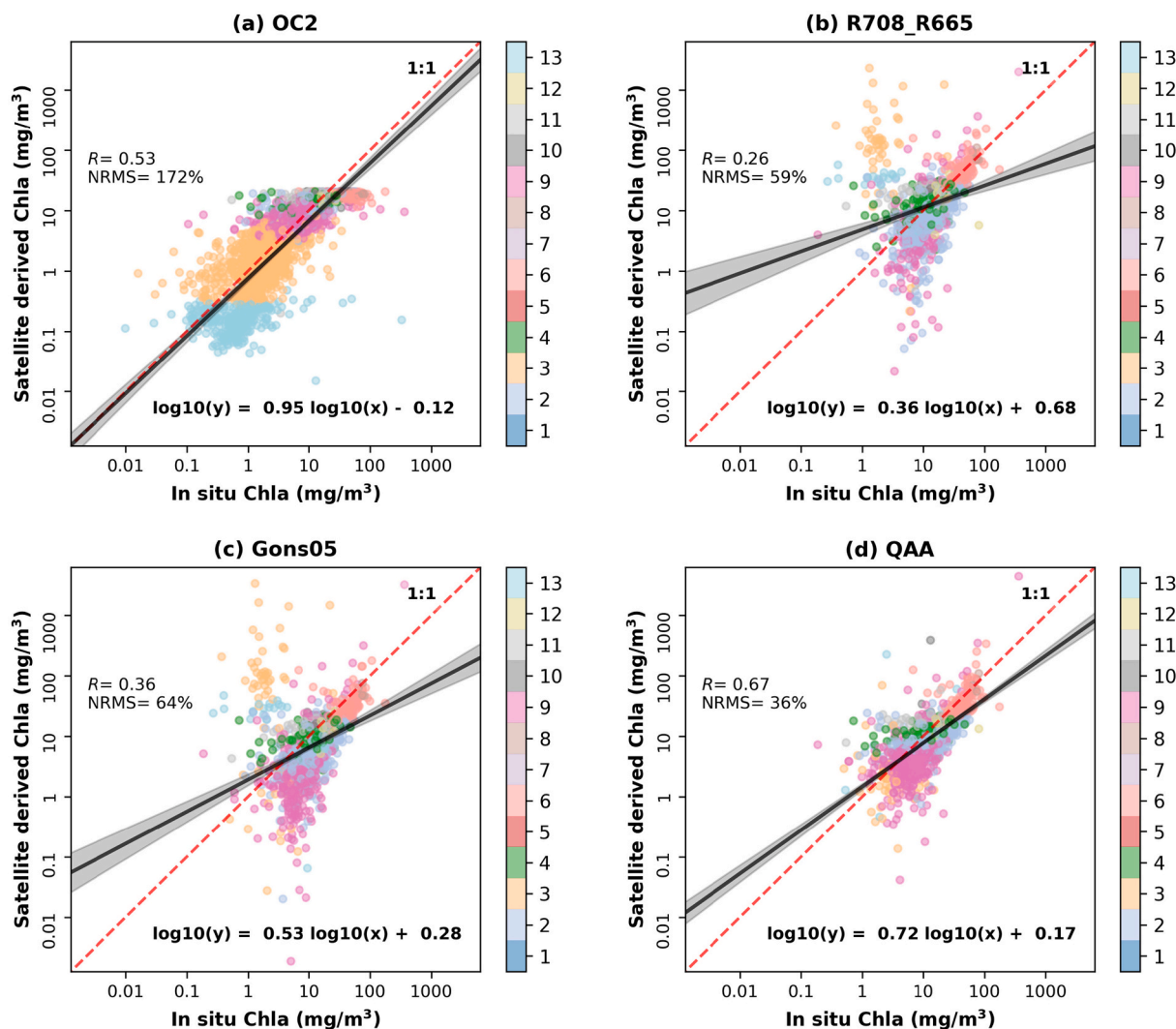
Fig. 6. Comparison between MERIS-derived and in situ chlorophyll-a concentration using the optimized (a) OC2, (b) R708_R665, (c) Gons05, and (d) QAA algorithms. The colour scale represents the predominant OWT.
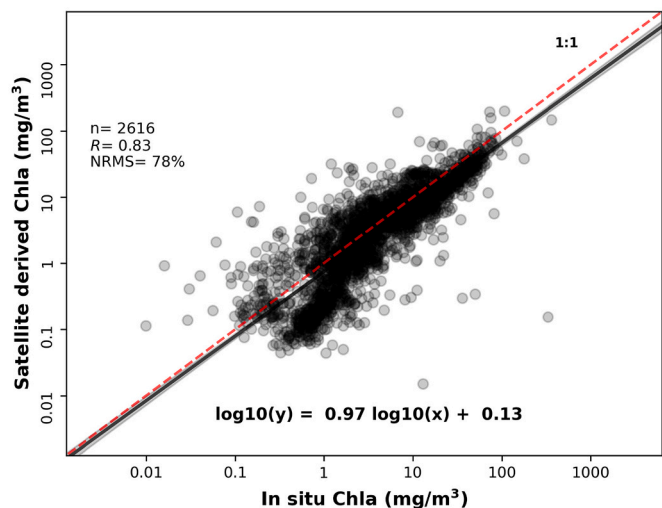

Fig. 7. Comparison between in situ and weighted blending chlorophyll-a derived from MERIS.

increased with S_{OWT}, indicating that increased association with OWT 13 and the associated algorithm has the undesirable effect of increased product uncertainty. This is explained by a relatively low number of very clear water observations being associated with tuning of the OC2 algorithm, and that a specific algorithm tuning for this OWT may be required. The models generally show a robust and flat response over a wide range of S_{OWT} values, indicating a wide application range of this scheme. A summary of the uncertainty models for the 13 OWTs and their applicable ranges can be found in Table 6.

3.4. Uncertainty product maps: applications to MERIS

The uncertainty models derived in the previous sections were applied to MERIS scenes over lakes Taihu (31 July 2010), Turkana (1 August 2011), Vänern (16 July 2006), and Vättern (16 July 2006) to generate the blended Chla product and associated product uncertainty map (Fig. 10b). Higher uncertainty values were systematically observed near land and in small water bodies, associated with lower overall OWT similarity scores caused by the influence of adjacent land on retrieved reflectance (Fig. 10, right panel). Generally, relatively lower uncertainties were found in lake Taihu, lake Turkana and lake Vänern compared to lake Vättern, as seen in Fig. 10 (right panel), which is consistent with lower Chla concentrations and therefore expected (Fig. 10, left panel).
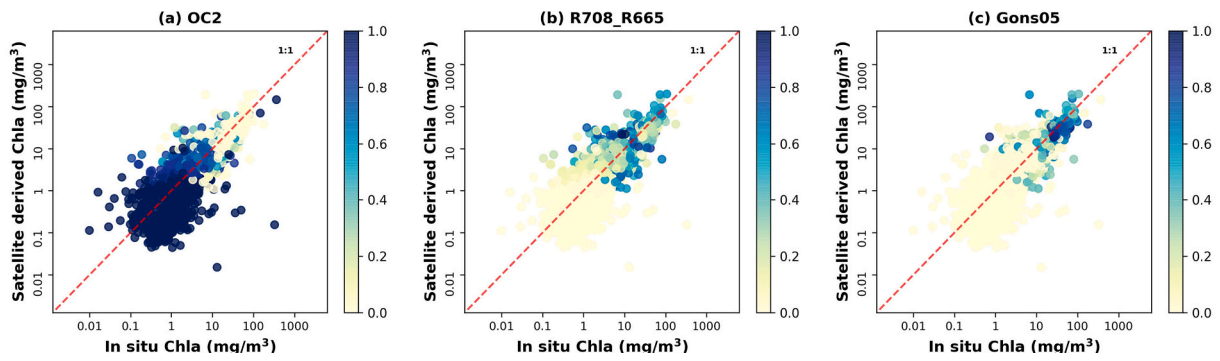
Fig. 8. Colour coded weighting factors of each algorithm in the blended chlorophyll-a product as shown in Fig. 7.
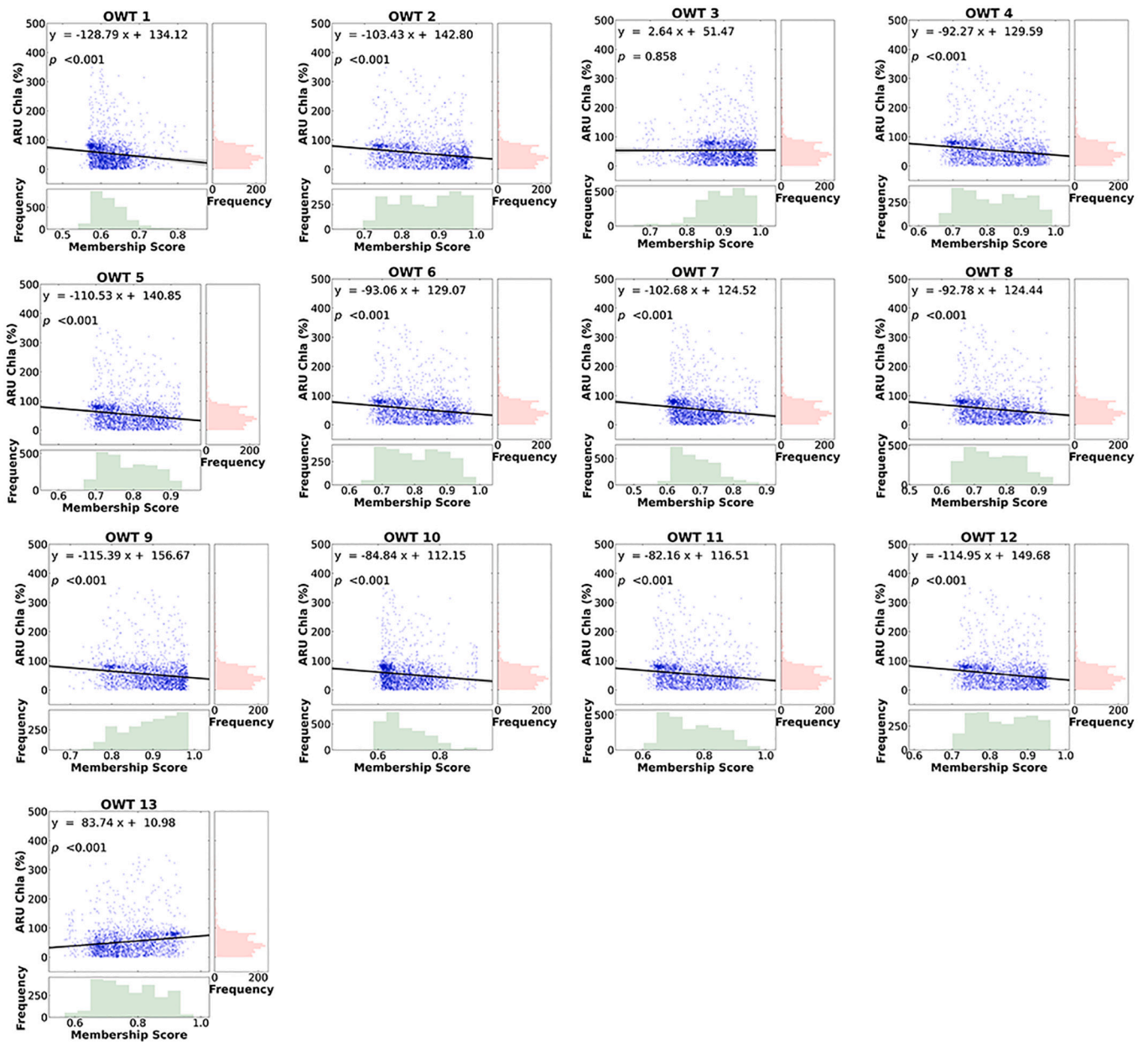

Fig. 9. Absolute Relative Uncertainty (ARU, %) model of blended chlorophyll-a for each OWT. The frequency distribution of the optical water type membership score (S_{OWT}, green bars) and ARU (red bars) are also shown in this figure. (For interpretation of the references to colour in this figure legend, the reader is referred to the web version of this article.)

Table 6
ARU uncertainty models and applicable range.

OWT	Slope	Intercept	p	Lower Boundary	Upper Boundary
1	−128.792	134.125	<0.001	0.453	0.916
2	−103.432	142.795	<0.001	0.573	1.182
3	2.639	51.465	=0.858	0.559	1.183
4	−92.275	129.594	<0.001	0.541	1.17
5	−110.532	140.846	<0.001	0.548	1.106
6	−93.063	129.069	<0.001	0.536	1.164
7	−102.68	124.517	<0.001	0.482	1.022
8	−92.783	124.443	<0.001	0.513	1.113
9	−115.388	156.672	<0.001	0.606	1.178
10	−84.838	112.148	<0.001	0.48	1.086
11	−82.16	116.513	<0.001	0.504	1.141
12	−114.947	149.679	<0.001	0.571	1.139
13	83.739	−10.978	<0.001	0.474	1.127

The Chla product and associated product uncertainty maps do not show artificial boundaries, suggesting that the blending of multiple algorithm outputs across water types performed as expected. To demonstrate the influence of each Chla algorithm on the final blended product, Fig. 11 shows the mapped weight distribution for the four Chla algorithms in the blended Chla products over lakes Taihu, Turkana, Vänern, and Vättern (on the same scenes as shown in Fig. 10). In turbid Lakes Taihu and Turkana, the weight of each algorithm shows distinct spatial gradients (Fig. 11a and b). For Lake Taihu, OC2 was weighted most heavily in southeast of the lake, corresponding to relatively clear waters; R708_R665 was weighted higher in the central east, Gons05 in the central west, and QAA in some northern bays (Fig. 11a). For Lake Turkana, OC2 had a prominent weight in the northern and southern areas, R708_R665 in the central lake, Gons05 in the central and northern lake, and QAA in small regions of northern lake (Fig. 11b). In the centre of lake Vänern, OC2 had the strongest weight (>0.4), followed by R708_R665, Gons05, and QAA (Fig. 11c). For Lake Vänern, in regions near land, the OC2 algorithm had the highest weight, followed by the Gons05 and QAA, and the R708_R665 had the smallest weight (Fig. 11c). In the oligotrophic clear Lake Vättern, the OC2 algorithm

accounted for >90% of the blended Chla product in the vast majority of the lake, while Gons05 and QAA exhibited relatively high weighting in some regions near land (Fig. 11d). The weight for R708_R665 in Lake Vättern is generally low across the whole lake (Fig. 11d).

3.5. Propagation from MERIS to OLCI

To assess the transferability of the proposed procedure from MERIS to OLCI, observations from two 3-year time periods were compared over four lakes with diverse optical properties and eutrophic states (Fig. 12). Chla for both sensors in the four lakes followed an approximately unimodal distribution. An increase in the median Chla concentration was observed between the observed MERIS and OLCI in Lake Taihu (from 12.5 to 17.4 mg/m^3), Turkana (from 3.8 to 5.3 mg/m^3), and Vänern (from 4.2 to 5.4 mg/m^3) as shown in Fig. 12a-c. In the oligotrophic Lake Vättern, the Chla distribution was similar between MERIS and OLCI (Fig. 12d). Generally, there was no major difference between MERIS and OLCI in the uncertainty distribution in each lake, indicating our procedure could be propagated to OLCI. The uncertainty for both MERIS and OLCI was highest in lake Vättern (56.6% and 56.4%), followed by lake Vänern (48.0% and 46.7%), Turkana (45.2% and 45.6%), and Taihu (40.6% and 40.2%).

4. Discussion

4.1. Implications for inland water remote sensing

4.1.1. The weighted blending procedure

The dataset of matching MERIS and in situ observations used in this study covers a wide range of eutrophication status of inland waters, from oligotrophic to hypereutrophic waters (Fig. 2). The striking variability in the bio-optical properties of inland waters, both regionally and temporally, makes it difficult, if not impossible, to generate a universally applicable algorithm to retrieve Chla concentration. In order to improve the accuracy of Chla estimates for optically complex waters, a number of studies highlighted the potential of an added OWT classification step
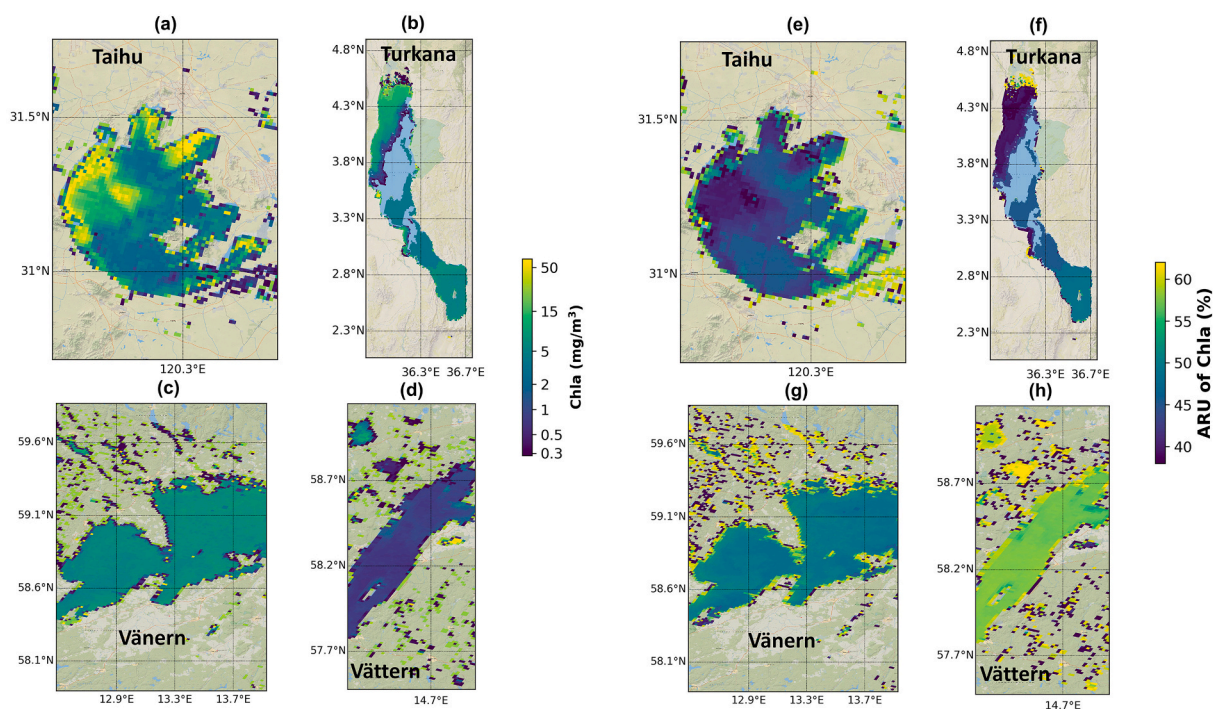

Fig. 10. Example maps of the weighted-blended chlorophyll-a product and its per-pixel Absolute Relative Uncertainty in lakes (a and e) Taihu, (b and f) Turkana, (c and g) Vänern, and (d and h) Vättern, including any small water bodies in their vicinity.
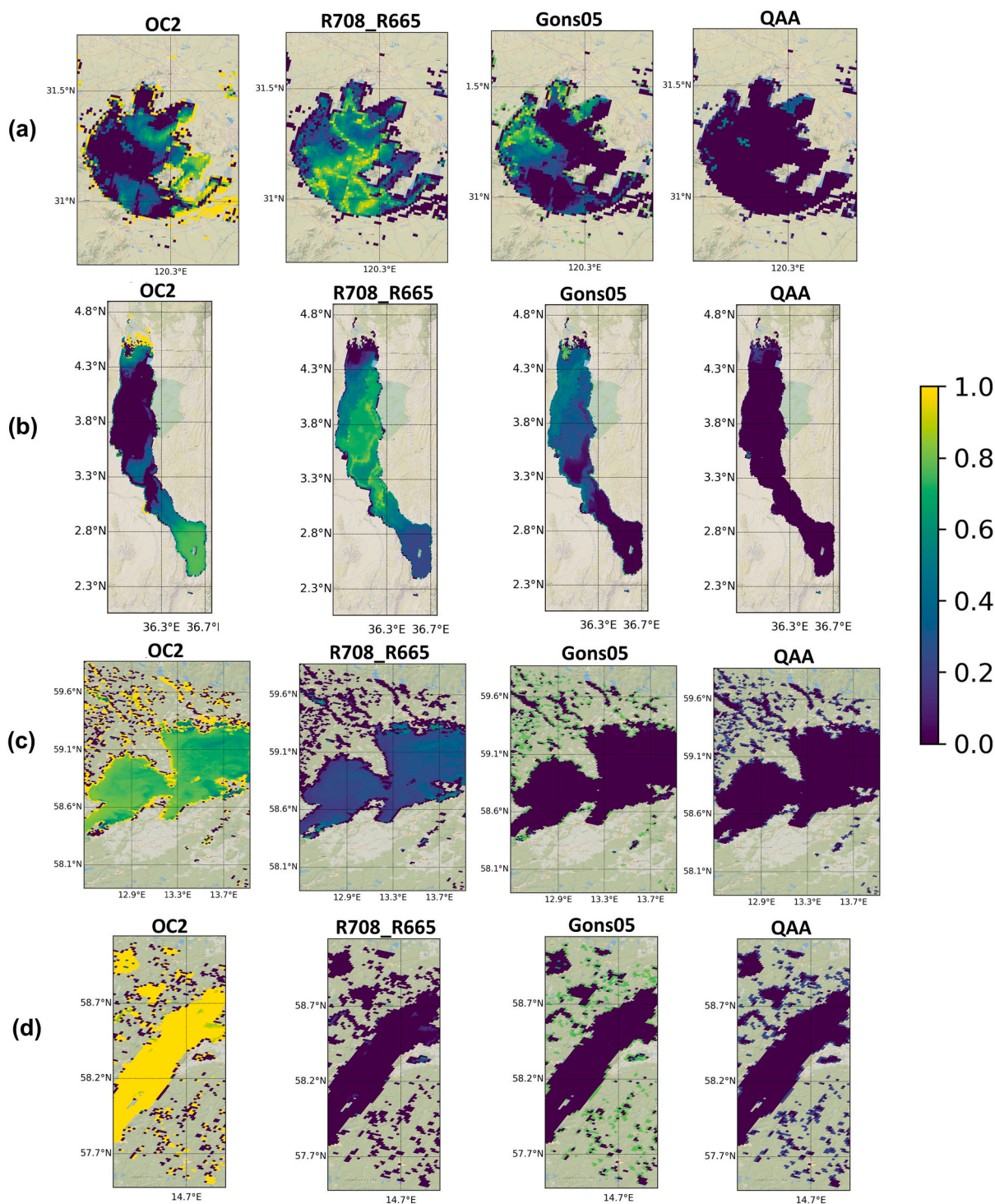
Fig. 11. Maps of the weight assigned to OC2, R708_R665, Gons05, and QAA in the blended chlorophyll-a product in lakes (a) Taihu, (b) Turkana, (c) Vänern, and (d) Vättern.

and subsequent type-specific algorithm development, regional tuning, or even algorithms switching (Moore et al., 2014; Neil et al., 2019; Vantrepotte et al., 2012).

Our assessment of a weighted blended Chla product procedure based on the fuzzy OWT classification framework shows significant improvement in the retrieval performance compared to that of individual regionally tuned algorithms (Fig. 6 and Fig. 7). This was somewhat expected based on the algorithm tuning exercise on in situ reflectance data by Neil et al. (2019) and the deployment of the individual algorithm to

suitable water bodies in their original publications. These results nevertheless show that the biases that are apparent in the matchup analysis of reflectance data can indeed be overcome in the present system of atmospheric correction and Chla retrieval algorithms, over a much wider range of water types than previously attempted with satellite data. In this dataset, it was found that these selected algorithms work adequately across several OWTs. This could be explained by the fact that the OWTs generalize the optical properties of natural waters, which is based on all optical components, not just Chla. Reciprocally, it
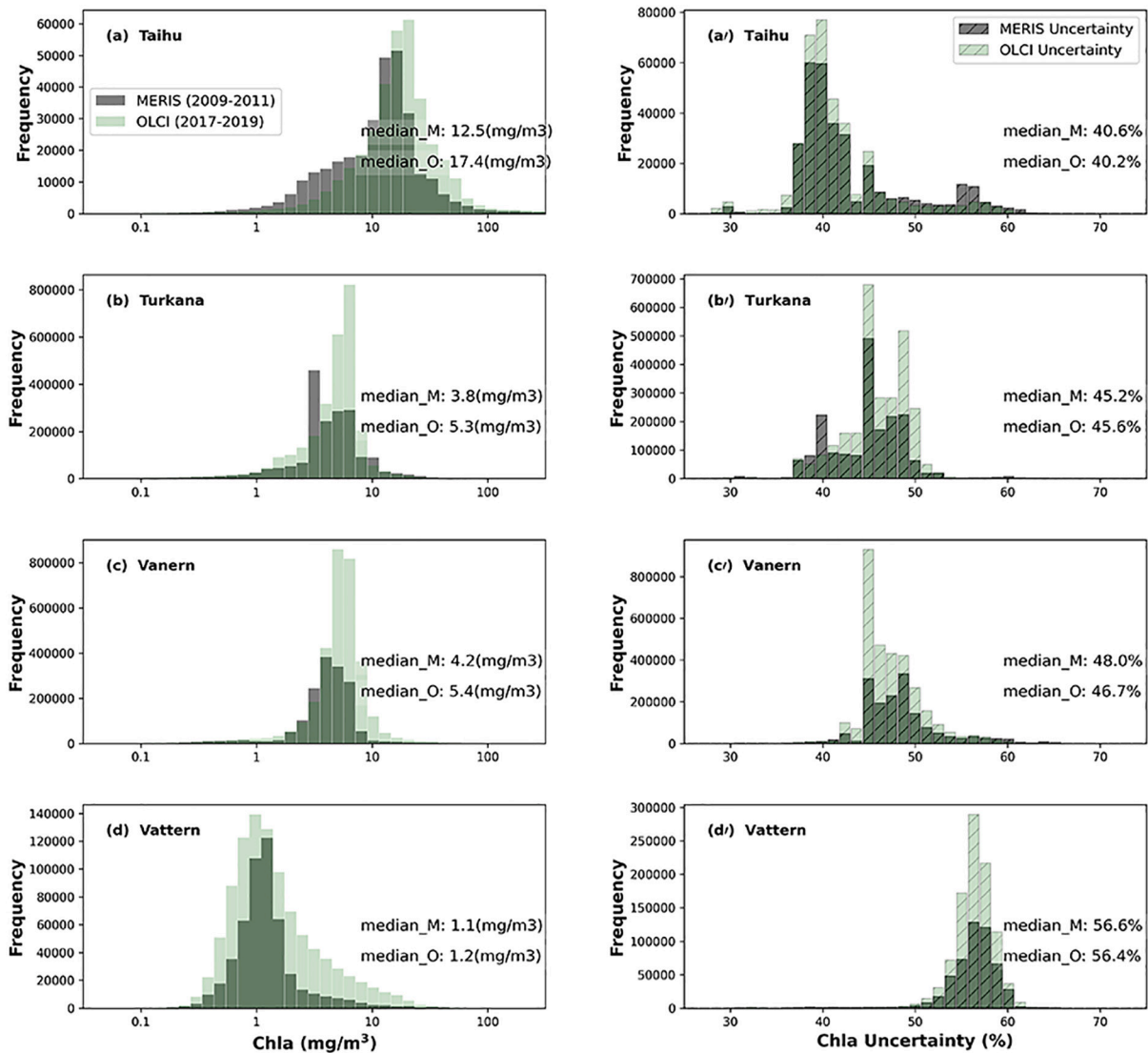
Fig. 12. Frequency distribution of chlorophyll-a and chlorophyll-a uncertainty in lakes Taihu, Turkana, Vänern and Vättern for MERIS (2009–2011) and OLCI (2017–2019).

is to be expected that one algorithm provides the best Chla estimate for more than one OWT, because the expression of Chla is similar between those OWTs whereas other components may differ. The application of the selected algorithms further confirms the scope of applicability of each algorithm, either in terms of the assignment to specific OWTs or a given Chla range. Thus, we found that when applied to satellite data, the OCx algorithms based on blue/green band ratios performed best in clear inland waters (O'Reilly et al., 2000), when Chla concentration is less than 10 mg/m^3 and for OWTs 3, 9 and 13, while OWT 10 did not show good performance although was assigned to OCx. The algorithms based on NIR-red ratios work expectedly better in more turbid and productive waters (Fig. 6) associated with Chla concentrations >10 mg/m^3 and Gons05 being most applicable to OWTs 4, 6, 10, and 11. The complementary algorithm performance underlines the optical complexity of inland waters and the difficulty in advocating a single 'classic' algorithm (as supposed to other switching techniques, or machine learning) for use in optically diverse waters. The wide applicability of the OWT based Chla retrieval is therefore evident. It is, however, worth noting that these results constitute are not a guarantee that these concentration estimates perform adequately in individual water bodies. The reason for this caveat is that the methodology is entirely based on pooled calibration of the available in situ data for each of the identified water types.

Further OWTs may need to be defined in future, as in situ reference observation data sets grow. However, the OWT membership weights do provide insight into whether a satellite observation corresponds to any of the defined water types, and further informs the characterization of product uncertainty for individual OWT-algorithm pairs discussed further below.

In this study, OWTs 1 and 7 (assigned to QAA) were not represented in the top-3 for the matchups in the blending procedure (Fig. 8), among which OWT 1 represents hypereutrophic waters with scums of cyanobacteria and vegetation-like reflectance, and OWT 7 delineates waters with particularly high values of Chla and cyanobacteria abundances (Spyrakos et al., 2018). This indicates that either those are rarely occurring water types in our matchup datasets, especially within the pixel resolution of MERIS, or atmospheric correction using POLYMER failed to return such results. A larger volume of in situ radiometric reference data than presently available will be critical to adequately address these potential shortcomings.

In the context of satellite applications, the procedure proposed in this study allows per-pixel assignment of the best-suited algorithms, both spatially and temporally, by performing the OWT classification on each separate observation (the satellite pixel). With four candidate algorithms mapped to 13 OWTs, blending the results for the top-3 ranking

OWTs is not expected to mix highly diverging algorithm results, whereas it is likely that near optical boundaries the blending outperforms any alternatives by shifting weights of one underlying algorithm to another. In the example products shown here, one Chla algorithm exhibits high weights in the lake center; while in the regions near land, where the optical water properties are more complex, the weight of each algorithm switches dynamically (Fig. 10 and Fig. 11). Moreover, the combination of OWT membership scores and product uncertainty can be used to determine which OWTs are poorly handled by the existing set of retrieval algorithms. There is evidence of such behavior in the present analysis, since higher product uncertainty was generally associated with lower OWT scores in the 12 OWTs out of 13, all of which were associated with optically complex environments (Table 3. Optical water types and their descriptions after Spyrakos et al. (2018) and Fig. 9). Meanwhile, for the end-user, it is important that dynamic algorithm selection and blending provides a natural transition along the continuum of optical conditions between optical environments, avoiding artificial boundaries between pixels in the Chla products. In a wider context, although the candidates of algorithms or classified OWTs could be changed (in other studies or even for different water quality parameters), the underlying methodology for uncertainty estimation is fully reproducible.

4.1.2. Uncertainty characterization

In this study, the majority of the OWTs show a slight decreasing trend of ARU with increasing S_{OWT}, indicating that the uncertainty decreases when the R_w spectra more closely resemble at least one of the 13 OWTs. The exception of OWT 13 could be explained by the fact that the OWT 13 represents clear blue water (Spyrakos et al., 2018), which is a less common case for inland water bodies (Fig. 9). A clear advantage of the approach given here is that all data points contribute to characterizing the performance of an algorithm as a function of its OWT memberships. When few representative samples exist in the dataset, this merely limits the applicable range of the uncertainty model, which is preferred over arbitrarily selecting data from the whole data set to assess the performance of an algorithm for a given water type. The algorithms and corresponding uncertainties presented here form a global assessment – locally, for a single lake the results could be better or worse than the average and this would not change the optimal configuration of the system nor the global assessment.

In this study, some specific upstream effects in the remotely sensed data generation may have been circumvented by using in situ Chla concentration data as primary reference in end-to-end product assessment. These effects include sensor degradation, or dependence on ancillary meteorological datasets in atmospheric correction of the at-sensor radiance. However, certain sources of uncertainty, which may or may not propagate to Chla estimates, may still be included in the type of end-to-end uncertainty analysis that we propose. These include the individual effects of atmospheric conditions (from direct measurements or algorithm-internal estimates of atmospheric optical thickness) or the goodness-of-fit of the atmospheric correction model, radiometric degradation (characterized over time using stable targets), distance to adjacent bright features, whether static (land) or moving (cloud), and finally the shape of the reflectance spectrum in bands that are not used in a given algorithm, but which may help explain performance in subtle ways. A study on the impact of signal-to-noise ratio (SNR) in a hyper-spectral sensor (HICO) indicates that improving the SNR of the sensor itself by reasonably modifying the sensor design would reduce estimation uncertainties in Chla by around 10% (Moses et al., 2012). Therefore, the uncertainty model proposed in this study is anticipated to evolve to include further relevant effects as soon as these can be quantified. For example, the land adjacency effect propagates to the Chla products depending on specific algorithm sensitivity effects, with longer wavebands most affected. This effect is not systematic in nature and thus expected to be reflected in product uncertainty. Including these effects can at first order use the known distance to land features, but also be expanded to take land albedo into account, and would require dedicated

study into the effects on algorithm performance. Certain observation effects are expected to influence the magnitude in uncertainties resulting from the atmospheric correction of the R_w signal, such as the optical pathlength to the target under variable angles. Due to the scarcity of reference data, we do not anticipate that this effect can be isolated any time soon. The ARU of the blended algorithm result shows a relatively flat response to the OWT membership scores (Fig. 9), which could be interpreted as the uncertainty model based on OWT membership having limited predictive power. While this is a valid interpretation, suggesting that additional explanatory variables should be sought to improve the prediction of uncertainty, this is also expected behavior since the Chla is a blended product of several pre-assigned algorithms, designed to make the blended results less dependent on membership score. A deviation from a flat response would indicate that one or more of the algorithms is being applied in a sub-optimal manner for the OWT in question, which is indeed observed in individual algorithms applied to the full dataset. Marked improvements in Chla retrieval are then observed when comparing the individual algorithms responses to the blending result (Fig. 6 and Fig. 7). The uncertainty models presented in this manuscript allow the remaining uncertainties after the blending procedure to be captured within this weighted-blending scheme using optical membership scores, and the ARU response between (rather than within) the OWTs show considerable differences. If a flat response were generally to be assumed, the uncertainty model could be simplified to represent a single ARU per OWT, following which the uncertainty could be approximated by weighted averaging of the ARU metrics and OWT membership scores for a given observation. The present model is decidedly more elaborate and is expected to be more widely applicable. Meanwhile, the results from LOOCV analysis show that the MAPE histograms heavily skewed to low MAPE with median values ranging from 28% to 35%, which confirm the models' robustness and availability to predict the ARU (Fig. S3). Besides, applications of the models near shore show relatively high uncertainties across lake types, exhibiting the protentional influences of land adjacencies (Fig. 10), and therefore further demonstrates the validity of the proposed models.

Several previous studies conducted assessment analysis in the framework of optical water types (Jackson et al., 2017; Mélin and Franz, 2014; Moore et al., 2009; Moore et al., 2014). Moore et al. (2009) were the first to attempt to map the uncertainty of MODIS-derived Chla from the OC3M algorithm in oceanic waters, using eight OWTs constructed primarily from in situ observations in NOMAD (NASA bio-Optical Marine Algorithm Dataset). Another study by the Ocean Colour Climate Change Initiative (ESA OC-CCI) adopted a similar approach (Jackson et al., 2017). A central assumption of these studies has been that the uncertainty of an algorithm for a specific OWT is only valid for observations with high S_{OWT} with respect to that OWT, and the final uncertainty product is represented as a weighted-average of the mean uncertainty for the top-ranking OWTs. This has the disadvantage that when insufficient data are available to define uncertainties for an OWT, the approach is no longer viable for the final products, and this data scarcity is highly relevant for inland water remote sensing.

4.2. Future outlook

The present weighted blending procedure as well as the uncertainty characterization approach are equally applicable to other water quality products (such as total suspended matter, turbidity, diffuse attenuation coefficient, etc.) as well as to other sensors. The assessment and the uncertainty propagation presented are based on MERIS, due to its long operation (2002−2012) and coincidence with matching in situ data in the LIMNADES database. Pending a follow-on analysis using OLCI on Sentinel-3, we consider that the similarities in radiometric performance and waveband configuration with MERIS would allow propagation of the present results to OLCI. Pending wider availability in in situ data coinciding with the OLCI sensors, initial analyses completed in the Copernicus Land Monitoring Service, which also uses the *Calimnos*

processing chain and algorithm configuration of this study, have shown that there is overall consistency between per-lake time series of Chla observed with MERIS and OLCI (Stelzer et al., 2020), and the consistency in uncertainty distribution between MERIS and OLCI in the four lakes further confirms this (Fig. 12). These findings support that the algorithms and uncertainty models for MERIS can, at least for the time being, be applied to both sensors. To fill the gap between MERIS and OLCI, independent validation of algorithms is expected to facilitate the application of this procedure to MODIS. Thus, it is anticipated that the results of this research could be transferred to OLCI and MODIS such that an uninterrupted global inland water quality data set can be generated. Per-pixel uncertainty estimates form an essential component of such a dataset, because MODIS lacks some of the optical configuration of MERIS and OLCI that have led to the first globally successful application of these sensors to inland waters. Thus, per-pixel uncertainty products would help guide the selection and use of products from each of these sensors, particularly where their observation records overlap.

In addition to reliable water constituent retrieval algorithms and consistent methods for uncertainty estimation, accurate atmospheric correction remains highly desirable for the remote sensing of inland optical water quality. In a recent assessment of atmospheric correction methods for Landsat-8 and Sentinel-2 in inland waters (Pahlevan et al., 2021), different atmospheric correction methods were recommended based on per band, per OWT performances, indicating that so far there is no single solution, and a preferred atmospheric correction processor may be chosen according to the specific scientific objective and application. Our study indicates that even with ocean colour sensors, with better radiometric performance and a wider band set, the atmospheric correction results are still far removed from the performance observed in equivalent ocean studies (Fig. 5). The unfortunate reality is that atmospheric correction of inland water bodies, particularly when applied across the globe is both imperfect and difficult to validate. In other words, there is high uncertainty regarding the uncertainty estimates, due to limited in situ radiometric reference data. We believe this situation is gradually improving, but it will take time before the research community can successfully and efficiently address the issue of suboptimal atmospheric correction over inland waterbodies. We show that of the available codes, POLYMER performs (relatively) well in general, whilst the much better performing retrieval of Chla suggests (1) that the POLYMER R_w product bias is indeed mostly systematic, and (2) the best-performing Chla retrieval algorithms may effectively be cancelling out some of the problems that are poorly resolved during the prior atmospheric correction step.

In a broader perspective, this approach could also be extended to other sensors, atmospheric correction algorithms, and water quality parameters, and the approach proposed here can be used as a template to guide the algorithm selection and product evaluation. Hybrid processing systems that use TOA, bottom-of-rayleigh as well as atmospherically corrected observation data could be considered within the same OWT based framework. Finally, with a growing in situ dataset and associated observations of the inherent optical properties of water bodies, it may become feasible to further separate the matchups based on optical water types, generate additional types, and identify new research horizons for water quality retrieval algorithms in inland waters.

5. Conclusions

This study aimed to introduce a framework for generating per-pixel product uncertainty for Chla and associated products from satellite observations in optically complex inland waters. Four Chla algorithms were included from previous round-robin comparison and algorithm coefficient optimization (Neil et al., 2019) and assignment to 13 OWTs (Spyrakos et al., 2018). Weighted blending of the Chla products based on similarities to these OWTs showed dramatic improvement in performance compared to that of the individual algorithms within the available MERIS matchups. This study confirms the benefit of the OWT framework to handle the wide Chla concentration range encountered in optically diverse inland waters. Within this framework, an uncertainty estimation model was developed to propagate algorithm uncertainties to per-pixel uncertainty maps. This study contributes a crucial step for the uptake of inland water quality remote sensing in limnology and specifically the global assessment of environmental change in optically diverse inland waters.

Declaration of Competing Interest

The authors declare that they have no known competing financial interests or personal relationships that could have appeared to influence the work reported in this paper.

Acknowledgements

Appendix A. Appendix

(a) OC2 algorithm

The OC2 algorithm, originally formulated to retrieve Chla from relatively clear ocean waters where phytoplankton and other optically active substances covary, relies on a ratio of blue and green wavebands. The algorithm is formulated as:

$$log_{10}\left(Chla\left[mgm^{-3}\right]\right) = a_0 + \sum_{i=1}^{4} a_i \left(log_{10}\left(\frac{R_w(490)}{R_w(560)} \right) \right)^i \tag{A1}$$

where $a_0 = 0.1731$, $a_1 = -3.9630$, $a_2 = -0.5620$, $a_3 = 4.5008$ and $a_4 = -3.0020$ are tuned constants.

(b) R708_R665 algorithm

The Gilerson et al. (2010) algorithm is an empirically tuned ratio of bands 708 and 665 nm:

$$Chla\left[mg\ m^{-3}\right] = A \times ratio^B + C \tag{A2}$$

where $A = 76.62$, $B = 0.7393$ and $C = -54.99$ are tuning coefficients empirically calibrated against LIMNADES.

(c) Gons05 algorithm

The Gons et al. (2005) algorithm uses the same band ratio and additionally analytically retrieves the backscattering coefficient from the 778 nm band. Subsequently, the absorption at 665 nm is analytically retrieved by inverting the Gordon reflectance model and attributed to Chla and water. The algorithm is specified as follows:

$$Chla\left[mg\ m^{-3}\right] = \left[\left(\frac{R(709)}{R(665)}\right) \times (a_w(709) + b_b) - a_w(665) - b_b^P\right] \bigg/ a_{ph}^*(665) \tag{A3.1}$$

where $a_w(709) = 0.84784\ \text{m}^{-1}$ and $a_w(665) = 0.431138\ \text{m}^{-1}$ are absorption by water obtained from Röttgers et al. (2010). Further, $a^*_{ph}(665) = 0.025$ $\text{m}^2\,\text{mg}^{-1}$ is the Chla specific absorption coefficient tuned in our study. The empirical constant $P = 1.06$ was not changed from the original formulation. The backscattering coefficient b_b is considered spectrally neutral and derived from a single near infra-red waveband:

$$b_b = \frac{0.6 \times a_w(779) \times R_w(779)}{0.082 - 0.6 \times R_w(779)} \tag{A3.2}$$

(d) QAA

The (Mishra et al., 2013a; Mishra et al., 2013b) implementation of the QAA (Lee et al., 2014) derives the Chla product from the phytoplankton absorption at 665 nm as follows:

$$Chla\left[mg\ m^{-3}\right] = A \times a_{ph}(665)^B \tag{A4.1}$$

where $A = 63.375$ and $B = 0.442$. The $a_{ph}(665)$ is retrieved from a set of equations, accounting for non-phytoplankton absorption in this band through the interpretation of absorption in blue and green wavebands:

$$a_{ph}(665) = a(665) - a_w(665) - a_{ys}(665),\ a_{ys}(665) = a_{ys}(442)e^{-S_{CDOM}(665-442)},\ a_{ys}(442) = \frac{(a(412) - s_1 \times a(442)) - (a_w(412) - (e_1 \times a_w(412)))}{e_1 - s_1} \tag{A4.2}$$

where $a_w(412) = 0.004805$ and $a_w(665) = 0.4289$ (Röttgers et al., 2010), $S_{CDOM} = 0.0135\ \text{nm}^{-1}$ is the average exponential slope coefficient for yellow substances derived from LIMNADES, and e_1 and s_1 are defined as

$$s_1 = 0.74 + \frac{0.2}{0.8 + \frac{rrs(442)}{rrs(560)}},$$

$$e_1 = e^{S(442-412)}$$

where the absorption in bands 412, 442 and 665 nm is obtained as

$$a(\lambda) = \frac{(1.0 - u(\lambda)) \times (b_{bw}(\lambda) + b_b(\lambda))}{u(\lambda)}. \tag{A4.3}$$

Here, $b_{bw}(\lambda)$ is the backscattering coefficient of pure water obtained from Morel (1974) assuming zero salinity. In turn, $u(\lambda)$ is the ratio of backscattering to the sum of backscattering and absorption, which according to the work by Gordon et al. (1988) can be obtained from below-surface remote-sensing reflectance $rrs(\lambda)$ as:

$$u(\lambda) = \frac{-g_0 + \sqrt{g_0^2 + (4 \times g_1) \times rrs(\lambda)}}{2 \times g_1}, \tag{A4.4}$$

With $g_0 = 0.089$ and $g_1 = 0.125$. The rrs bands are obtained from $R_w(\lambda)$ using:

$$rrs(\lambda) = \frac{R_w(\lambda)}{\pi(0.52 + 0.54 \times R_w(\lambda))} \tag{A4.5}$$

References

Boyer, J.N., Kelble, C.R., Ortner, P.B., Rudnick, D.T., 2009. Phytoplankton bloom status: chlorophyll a biomass as an indicator of water quality condition in the southern estuaries of Florida, USA. Ecol. Indic. 9, S56–S67.

Brasseur, P., Gruber, N., Barciela, R., Brander, K., Doron, M., Elmoussaoui, A., Hobday, A.J., Huret, M., Kremeur, A.S., Lehodey, P., 2009. Integrating biogeochemistry and ecology into ocean data assimilation systems. Oceanogr. 22, 206–215.

Calmettes, B., Giardino, C., 2019. User requirement document (URD) for the lakes climate change initiative. Pp. 35.

Cao, Z., Ma, R., Duan, H., Pahlevan, N., Melack, J., Shen, M., Xue, K., 2020. A machine learning approach to estimate chlorophyll-a from Landsat-8 measurements in inland lakes. Remote Sens. Environ. 248, 111974.

Carlson, R.E., Simpson, J., 1996. A coordinator's Guide to Volunteer Lake Monitoring Methods. North American Lake Management Society, USA, p. 96.

Cole, G.A., Weihe, P.E., 2015. Textbook of Limnology. Waveland Press, Long Grove.

Dinguirard, M., Slater, P.N., 1999. Calibration of space-multispectral imaging sensors: a review. Remote Sens. Environ. 68, 194–205.

Downing, J.A., Prairie, Y., Cole, J., Duarte, C., Tranvik, L., Striegl, R.G., McDowell, W., Kortelainen, P., Caraco, N., Melack, J., 2006. The global abundance and size distribution of lakes, ponds, and impoundments. Limnol. Oceanogr. 51, 2388–2397.

Dudgeon, D., Arthington, A.H., Gessner, M.O., Kawabata, Z.I., Knowler, D.J., Lévêque, C., Naiman, R.J., Prieur-Richard, A.H., Soto, D., Stiassny, M.L., 2006. Freshwater biodiversity: importance, threats, status and conservation challenges. Biol. Rev. 81, 163–182.

Dutkiewicz, S., Hickman, A., Jahn, O., Gregg, W., Mouw, C., Follows, M., 2015. Capturing optically important constituents and properties in a marine biogeochemical and ecosystem model. Biogeosciences 12, 4447–4481.

Eleveld, M.A., Ruescas, A.B., Hommersom, A., Moore, T.S., Peters, S.W., Brockmann, C., 2017. An optical classification tool for global lake waters. Remote Sens. 9, 420.

Gilerson, A.A., Gitelson, A.A., Zhou, J., Gurlin, D., Moses, W., Ioannou, I., Ahmed, S.A., 2010. Algorithms for remote estimation of chlorophyll-a in coastal and inland waters using red and near infrared bands. Opt. Express 18, 24109–24125.

Gons, H.J., Rijkeboer, M., Ruddick, K.G., 2005. Effect of a waveband shift on chlorophyll retrieval from MERIS imagery of inland and coastal waters. J. Plankton Res. 27, 125–127.

Gordon, H.R., Wang, M., 1992. Surface-roughness considerations for atmospheric correction of ocean color sensors. II: Error in the retrieved water-leaving radiance. Appl. Opt. 31, 4261–4267.

Gordon, H.R., Brown, O.B., Evans, R.H., Brown, J.W., Smith, R.C., Baker, K.S., Clark, D. K., 1988. A semianalytic radiance model of ocean color. J. Geophys. Res. Atmos. 93, 10909–10924.

Guanter, L., Ruiz-Verdú, A., Odermatt, D., Giardino, C., Simis, S., Estellés, V., Heege, T., Domínguez-Gómez, J.A., Moreno, J., 2010. Atmospheric correction of ENVISAT/ MERIS data over inland waters: validation for European lakes. Remote Sens. Environ. 114, 467–480.

Harmel, T., Chami, M., 2011. Influence of polarimetric satellite data measured in the visible region on aerosol detection and on the performance of atmospheric correction procedure over open ocean waters. Opt. Express 19, 20960–20983.

Henson, S.A., Raitsos, D., Dunne, J.P., McQuatters-Gollop, A., 2009. Decadal variability in biogeochemical models: comparison with a 50-year ocean colour dataset. Geophys. Res. Lett. 36.

IOCCG, 2010. Atmospheric correction for remotely-sensed ocean-colour products. IOCCG report series. IOCCG, Dartmouth. Canada. 10, 5–12.

IOCCG, 2019. Uncertainties in Ocean Colour Remote Sensing. IOCCG Report Series Dartmouth, Canada, pp. 1–137.

Jackson, T., Sathyendranath, S., Mélin, F., 2017. An improved optical classification scheme for the ocean colour essential climate variable and its applications. Remote Sens. Environ. 203, 152–161.

Karydis, M., Kitsiou, D., 2019. Marine Eutrophication: A Global Perspective. CRC Press, Boca Raton.

Kirk, J.T.O., 2011. Light and Photosynthesis in Aquatic Ecosystems, 3nd ed. Cambridge University Press, New York.

Kravitz, J., Mark, M., Lain, L., Stewart, B., Sarah, F., 2021. Potential for high fidelity global mapping of common inland water quality products at high spatial and temporal resolutions based on a synthetic data and machine learning approach. Front. Environ. Sci. https://doi.org/10.3389/fenvs.2021.587660.

Kromkamp, J.C., Van Engeland, T., 2010. Changes in phytoplankton biomass in the Western Scheldt estuary during the period 1978–2006. Estuaries Coast. 33, 270–285.

Kruse, F.A., Lefkoff, A., Boardman, J., Heidebrecht, K., Shapiro, A., Barloon, P., Goetz, A., 1993. The spectral image processing system (SIPS)-interactive visualization and analysis of imaging spectrometer data. In: AIP Conf. Proc. American Institute of Physics, pp. 192–201.

Lee, Z., Lubac, B., Werdell, J., Arnone, R., 2014. Update of the Quasi-Analytical Algorithm (QAA_v6). International Ocean Color Group Software Report.

Liu, X., Zhang, Y., Yin, Y., Wang, M., Qin, B., 2013. Wind and submerged aquatic vegetation influence bio-optical properties in large shallow Lake Taihu. China. J. Geophys. Res. Biogeosci. 118, 713–727.

Matthews, M.W., Bernard, S., Robertson, L., 2012. An algorithm for detecting trophic status (chlorophyll-a), cyanobacterial-dominance, surface scums and floating vegetation in inland and coastal waters. Remote Sens. Environ. 124, 637–652.

Mélin, F., Franz, B.A., 2014. Assessment of satellite ocean colour radiometry and derived geophysical products. Experimental Methods in the Physical Sciences. Elsevier, pp. 609–638.

Merchant, C.J., Paul, F., Popp, T., Ablain, M., Bontemps, S., Defourny, P., Hollmann, R., Lavergne, T., Laeng, A., De Leeuw, G., 2017. Uncertainty information in climate data records from earth observation. Earth Syst. Sci. Data 9, 511–527.

Mishra, S., Mishra, D.R., Lee, Z., 2013a. Bio-optical inversion in highly turbid and cyanobacteria-dominated waters. IEEE Trans. Geosci. Remote Sens. 52, 375–388.

Mishra, S., Mishra, D.R., Lee, Z., Tucker, C.S., 2013b. Quantifying cyanobacterial phycocyanin concentration in turbid productive waters: a quasi-analytical approach. Remote Sens. Environ. 133, 141–151.

Moore, T.S., Campbell, J.W., Dowell, M.D., 2009. A class-based approach to characterizing and mapping the uncertainty of the MODIS Ocean chlorophyll product. Remote Sens. Environ. 113, 2424–2430.

Moore, T.S., Dowell, M.D., Bradt, S., Verdu, A.R., 2014. An optical water type framework for selecting and blending retrievals from bio-optical algorithms in lakes and coastal waters. Remote Sens. Environ. 143, 97–111.

Morel, A., 1974. Optical properties of pure water and pure sea water, Chap. 1. In: Jerlov, Nielsen (Eds.), Optical Aspects of Oceanography. Academic Press, New York, pp. 1–24.

Morel, A., Prieur, L., 1977. Analysis of variations in ocean color. Limnol. Oceanogr. 22, 709–722.

Moses, W.J., Bowles, J.H., Lucke, R.L., Corson, M.R., 2012. Impact of signal-to-noise ratio in a hyperspectral sensor on the accuracy of biophysical parameter estimation in case II waters. Opt. Express 20, 4309–4330.

Moses, W.J., Saprygin, V., Gerasyuk, V., Povazhnyy, V., Berdnikov, S., Gitelson, A.A., 2019. OLCI-based NIR-red models for estimating chlorophyll-a concentration in productive coastal waters—a preliminary evaluation. Environ. Res. Commun. 1, 011002.

Mueller, J.L., Fargion, G.S., 2002. Ocean Optics Protocols for Satellite Ocean Color Sensor Validation, Revision 3. National Aeronautics and Space Administration, Goddard Space Flight Center.

Neil, C., Spyrakos, E., Hunter, P.D., Tyler, A.N., 2019. A global approach for chlorophyll-a retrieval across optically complex inland waters based on optical water types. Remote Sens. Environ. 229, 159–178.

Nerger, L., Gregg, W.W., 2007. Assimilation of SeaWiFS data into a global ocean-biogeochemical model using a local SEIK filter. J. Mar. Syst. 68, 237–254.

O'Reilly, J.E., Maritorena, S., Mitchell, B.G., Siegel, D.A., Carder, K.L., Garver, S.A., Kahru, M., McClain, C., 1998. Ocean color chlorophyll algorithms for SeaWiFS. J. Geophys. Res. Oceans. 103, 24937–24953.

Pahlevan, N., Smith, B., Schalles, J., Binding, C., Cao, Z., Ma, R., Alikas, K., Kangro, K., Gurlin, D., Hà, N., 2020. Seamless retrievals of chlorophyll-a from Sentinel-2 (MSI) and Sentinel-3 (OLCI) in inland and coastal waters: a machine-learning approach. Remote Sens. Environ. 240, 111604.

O'Reilly, J.E., Maritorena, S., Siegel, D.A., O'Brien, M.C., Toole, D., Mitchell, B.G., Kahru, M., Chavez, F.P., Strutton, P., Cota, G.F., 2000. Ocean Color Chlorophyll a Algorithms for SeaWiFS, OC2, and OC4: Version 4. SeaWiFS postlaunch calibration validation analyses, Part 3, pp. 9–23.

Pahlevan, N., Mangin, A., Balasubramanian, S.V., Smith, B., Alikas, K., Arai, K., Barbosa, C., Bélanger, S., Binding, C., Bresciani, M., 2021. ACIX-aqua: a global assessment of atmospheric correction methods for Landsat-8 and Sentinel-2 over lakes, rivers, and coastal waters. Remote Sens. Environ. 258, 112366.

Palmer, S.C., Odermatt, D., Hunter, P., Brockmann, C., Presing, M., Balzter, H., Tóth, V., 2015. Satellite remote sensing of phytoplankton phenology in Lake Balaton using 10 years of MERIS observations. Remote Sens. Environ. 158, 441–452.

Röttgers, R., Doerfer, R., McKee, D., Schönfeld, W., 2010. Pure water spectral absorbtion, scattering, and real part of refractive index model. ESA algorithm technical basis document 1–18.

Shi, K., Li, Y., Li, L., Lu, H., 2013. Absorption characteristics of optically complex inland waters: implications for water optical classification. J. Geophys. Res. Biogeosci. 118, 860–874.

Shi, K., Zhang, Y., Liu, X., Wang, M., Qin, B., 2014. Remote sensing of diffuse attenuation coefficient of photosynthetically active radiation in Lake Taihu using MERIS data. Remote Sens. Environ. 140, 365–377.

Simis, S.G.H., Liu, X., Cretaux, J.F., Yesou, H., Malnes, E., Vickers, H., Blanco, P., Merchant, C.J., Carrea, L., Duguay, C., 2020a. Product validation and algorithm selection report (PVASR) and algorithm development plan (ADP). CCI-LAKES-0026-PVASR-ADP, pp. 23–26.

Simis, S.G.H., Stelzer, K., Müller, D., Selmes, N., 2020b. Copernicus global land operations "cryosphere and water" algorithm theoretical basis document: Lake waters 300m and 1km products, versions 1.3.0-1.4.0. CGLOPS2_ATBD_LWQ300_1km _v1.3.1_I1.12, pp. 1–46.

Spyrakos, E., Vilas, L.G., Palenzuela, J.M.T., Barton, E.D., 2011. Remote sensing chlorophyll a of optically complex waters (rias Baixas, NW Spain): application of a regionally specific chlorophyll a algorithm for MERIS full resolution data during an upwelling cycle. Remote Sens. Environ. 115, 2471–2485.

Spyrakos, E., O'Donnell, R., Hunter, P.D., Miller, C., Scott, M., Simis, S.G., Neil, C., Barbosa, C.C., Binding, C.E., Bradt, S., 2018. Optical types of inland and coastal waters. Limnol. Oceanogr. 63, 846–870.

Steinmetz, F., Deschamps, P.-Y., Ramon, D., 2011. Atmospheric correction in presence of sun glint: application to MERIS. Opt. Express 19, 9783–9800.

Stelzer, K., Müller, D., Simis, S.G.H., Selmes, N., 2020. Copernicus global land operations "cryosphere and water" quality assessment report - Lake water quality 300m and 1km products. CGLOPS2_QAR_LWQ300_1km_V1.3.1_I1.11, pp. 1–63.

Tibshirani, R., Walther, G., Hastie, T., 2001. Estimating the number of clusters in a data set via the gap statistic. J. R. Stat. Soc. Ser. B 63, 411–423.

Vantrepotte, V., Loisel, H., Dessailly, D., Mériaux, X., 2012. Optical classification of contrasted coastal waters. Remote Sens. Environ. 123, 306–323.

Verpoorter, C., Kutser, T., Seekell, D.A., Tranvik, L.J., 2014. A global inventory of lakes based on high-resolution satellite imagery. Geophys. Res. Lett. 41, 6396–6402.

Warren, M.A., Simis, S.G.H., Martinez-Vicente, V., Poser, K., Bresciani, M., Alikas, K., Spyrakos, E., Giardino, C., Ansper, A., 2019. Assessment of atmospheric correction algorithms for the sentinel-2A MultiSpectral imager over coastal and inland waters. Remote Sens. Environ. 225, 267–289.